Oncogene (2014) 33, 2273–2278

www.nature.com/onc

SHORT COMMUNICATION

ANGPTL4 is a secreted tumor suppressor that inhibits angiogenesis

E Okochi-Takada[1], N Hattori[1], T Tsukamoto[2], K Miyamoto[3], T Ando[1,4], S Ito[5], Y Yamamura[5], M Wakabayashi[1], Y Nobeyama[1,6] and T Ushijima[1]

Tumor suppressors with extracellular function are likely to have advantages as targets for cancer therapy, but few are known. Here, we focused on angiopoietin-like 4 (ANGPTL4), which is a secreted glycoprotein involved in lipoprotein metabolism and angiogenesis, is methylation-silenced in human cancers, but has unclear roles in cancer development and progression. We found a deletion mutation in its coiled-coil domain at its N-terminal in human gastric cancers, in addition to hypermethylation of the *ANGPTL4* promoter CpG islands. Forced expression of wild-type *ANGPTL4*, but not *ANGPTL4* with the deletion, at physiological levels markedly suppressed *in vivo* tumorigenicity and tumor angiogenesis, indicating that the latter caused the former. Tumor-derived ANGPTL4 suppressed *in vitro* vascular tube formation and proliferation of human umbilical vascular endothelial cells, partly due to suppression of ERK signaling. These showed that ANGPTL4 is a genetically and epigenetically inactivated secreted tumor suppressor that inhibits tumor angiogenesis.

Oncogene (2014) **33,** 2273–2278; doi:10.1038/onc.2013.174; published online 20 May 2013

Keywords: epigenetics; angiogenesis; tumor suppressor; gastric cancer; DNA methylation

INTRODUCTION

Tumor-suppressor genes (TSGs) are somatically inactivated by genetic and/or epigenetic mechanisms.[1,2] Targeting TSGs for molecular target therapy has been attempted mainly for *p53*.[3,4] However, the attempts have not been easy, partly due to the fact that the *p53* gene product is neither a cell surface protein nor a typical enzyme.[5] Considering efficient delivery to targets, TSGs whose products function extracellularly as secreted proteins are likely to have advantages. So far, secreted frizzled-related proteins are known as secreted tumor suppressors,[6,7] but few others are known.

As a candidate, we previously identified that angiopoietin-like 4 (*ANGPTL4*), a member of the angiopoietin-like family, was silenced by aberrant DNA methylation of promoter CpG islands (CGIs) (methylation-silenced) in human cancers.[8,9] ANGPTL4 is a secreted glycoprotein, and is involved in lipoprotein metabolism through inhibition of lipoprotein lipase.[10] In contrast, the role of ANGPTL4 in angiogenesis remains controversial.[11–15] Likewise, its role in tumor formation also remains controversial—some reports suggesting its tumor-suppressive function[12,16,17] and others its oncogenic function.[18–20]

Here, we aimed to clarify the role of ANGPTL4 in cancer development and progression and also in tumor angiogenesis.

RESULTS AND DISCUSSION

Inactivation of *ANGPTL4* by epigenetic and genetic mechanisms in human gastric cancers

ANGPTL4 methylation was detected in 10 of 91 human gastric cancers (11%) by quantitative real-time methylation-specific PCR (Figure 1a). The mRNA and protein expression levels of ANGPTL4 in cancers with *ANGPTL4* methylation were significantly lower than those in cancers without methylation (Supplementary Figure S2). Methylation status did not have any association with clinicopathological features, but had a significant association with Epstein-Barr virus infection status and the presence of the CGI methylator phenotype[21] (Supplementary Figure S1 and Supplementary Table S1). In non-cancerous gastric mucosae of 71 gastric cancer patients and gastric mucosae of 58 healthy volunteers, the methylation level was also quantified. It was significantly higher in cancer patients than in healthy volunteers and in individuals with *H. pylori* infection than in those without (Figure 1b). This suggested the potential involvement of *ANGPTL4* methylation in the formation of an epigenetic field for canceriza-tion, a predisposed normal-appearing tissue.[22]

ANGPTL4 mutation was then analyzed in 89 of the 91 gastric cancers (due to sample availability), and a somatic 21-bp deletion in exon 1 was identified in one specimen (cancer #217T) without *ANGPTL4* methylation (Figures 1c and d). ANGPLT4 consists of an N-terminal coiled-coil domain (CCD) and a C-terminal fibrinogen-like domain,[23,24] and the 21-bp deletion was located in the CCD (Supplementary Figure S3). The CCD is reported to be critical for regulation of the anti-angiogenic activity of ANGPTL4,[13] and the deletion here involved one of the two cysteine residues (Cys76 and Cys80) essential for the activity regulation by oligomerization.[25,26]

Loss of heterozygosity (LOH), which suggests the presence of a TSG,[27] was detected in 4 of 16 samples (25%) informative for a C/T polymorphism at the second position of codon 266. The locus of

[1]Division of Epigenomics, National Cancer Center Research Institute, Tokyo, Japan; [2]Oncological Pathology Division, Aichi Cancer Center Research Institute, Nagoya, Japan; [3]Division of Molecular Oncology, National Hospital Organization Kure Medical Center and Chugoku Cancer Center, Kureshi, Japan; [4] Third Department of Internal Medicine, University of Toyama, Toyama, Japan; [5]Department of Gastroenterological Surgery, Aichi Cancer Center Central Hospital, Nagoya, Japan and [6]Department of Dermatology, The Jikei University School of Medicine, Tokyo, Japan. Correspondence: Dr T Ushijima, Division of Epigenomics, National Cancer Center Research Institute, 5-1-1 Tsukiji, Chuo-ku, Tokyo 104-0045, Japan.
E-mail: tushijim@ncc.go.jp
Received 27 September 2012; revised 14 February 2013; accepted 28 March 2013; published online 20 May 2013

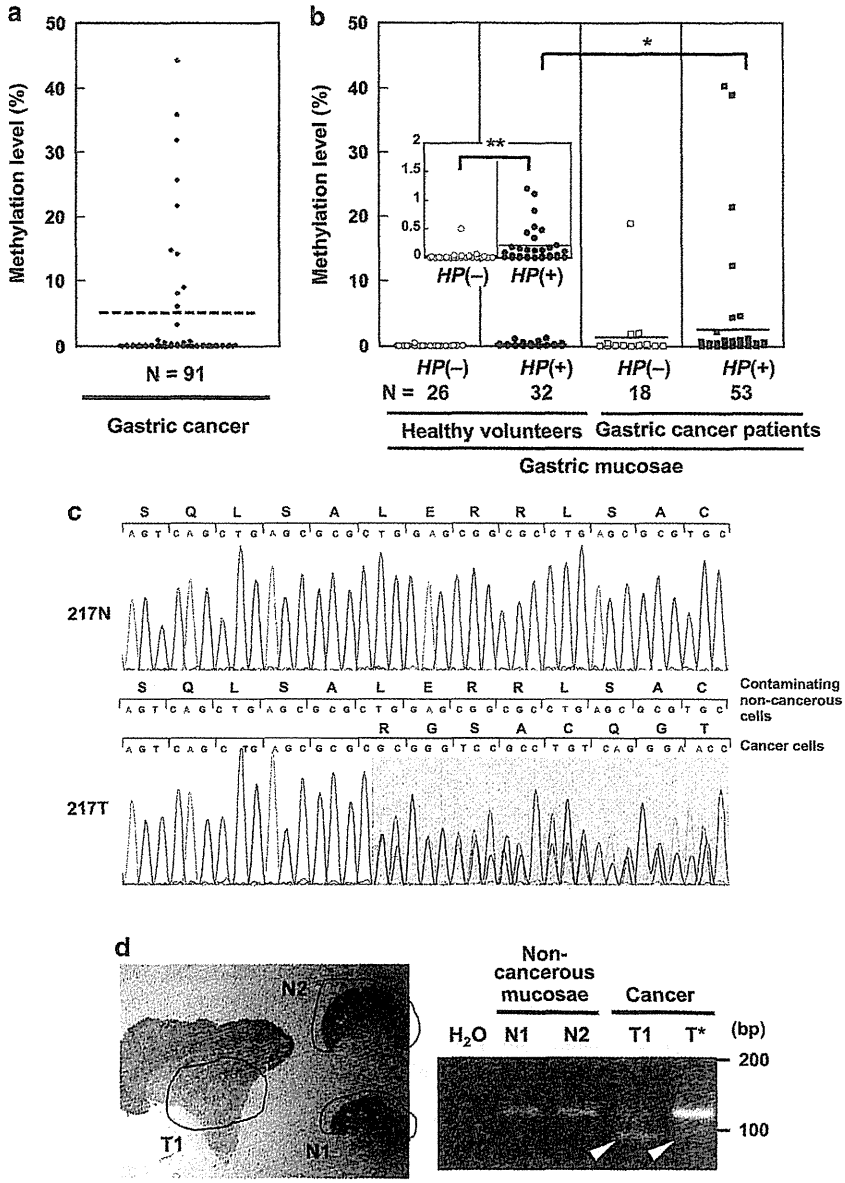

Figure 1. Aberrant methylation and a mutation of *ANGPTL4* in human gastric cancers, and methylation in non-cancerous gastric mucosae. (**a**) *ANGPTL4* methylation levels in gastric cancer specimens. Cancer samples were obtained from 91 gastric cancer patients undergoing gastrectomy with informed consents and approval by the institutional review boards. Some of the samples and methylation data were obtained from our previous study.[33] Quantitative real-time methylation-specific PCR was conducted with sodium bisulfite-treated DNA and primer sets specific to methylated and unmethylated sequences (Supplementary Table S2). Using a cutoff value of 6% (broken line), as in previous studies,[34–36] 10 cancer specimens were considered to have aberrant methylation. (**b**) *ANGPTL4* methylation levels in gastric mucosae of 58 healthy volunteers (30 male and 28 female; average age = 55 years) and 71 non-cancerous gastric mucosae of gastric cancer patients (50 male and 21 female; average age = 67 years) obtained by endoscopic biopsy of the antral region. *H. pylori* infection status was analyzed by a serum anti-*H. pylori* IgG antibody test (SRL, Tokyo, Japan), rapid urease test (Otsuka, Tokushima, Japan) or culture test (Eiken, Tokyo, Japan). The methylation level in gastric mucosae was significantly higher in gastric cancer patients than in healthy volunteers. The mean methylation level is shown by a horizontal line. $^{*}P<0.05$, $^{**}P<0.01$ (the unpaired Welch's *t*-test, two-sided). (**c**) A deletion mutation in a human gastric cancer specimen. All the seven exons and splice donor/acceptor sites of *ANGPTL4* were amplified by PCR (Supplementary Table S2), and the PCR products were directly cycle sequenced. The sequences of a gastric cancer specimen (217T) and its corresponding non-cancerous tissue (217N) between nucleotides 385 and 423 are shown. A 21-bp deletion in exon 1 was detected (shown in the gray background). (**d**) Confirmation of the deletion mutation using DNA samples obtained from a single tissue section. A 117-bp region encompassing the deletion was amplified by PCR, and the deletion was detected as a PCR product with a shorter size (96 bp). DNA from the cancer (T1), but not that from non-cancerous areas (N1 and N2), yielded the shorter product (shown by arrows). T*, genomic DNA extracted from frozen tumor tissues. If LOH was present in T1, the band intensity ratio was expected to be 1:1 (wild type:deletion mutant) (fraction of cancer cells was pathologically assessed to be 61–67%). If LOH was not present, it was expected to be 2:1. The ratio observed was ~1:2, and LOH was considered to be present in T1.

ANGPTL4, 19p13.3, has been suggested to contain TSGs, due to frequent LOH of the region in several types of cancers, such as pancreatic and colon cancers.[28–30] In addition, two human gastric cancer cell lines (MKN28 and AGS) without *ANGPTL4* expression had methylation of its promoter, and their treatment with 5-aza-2′-deoxycytidine (5-aza-dC), a DNA methylation inhibitor,

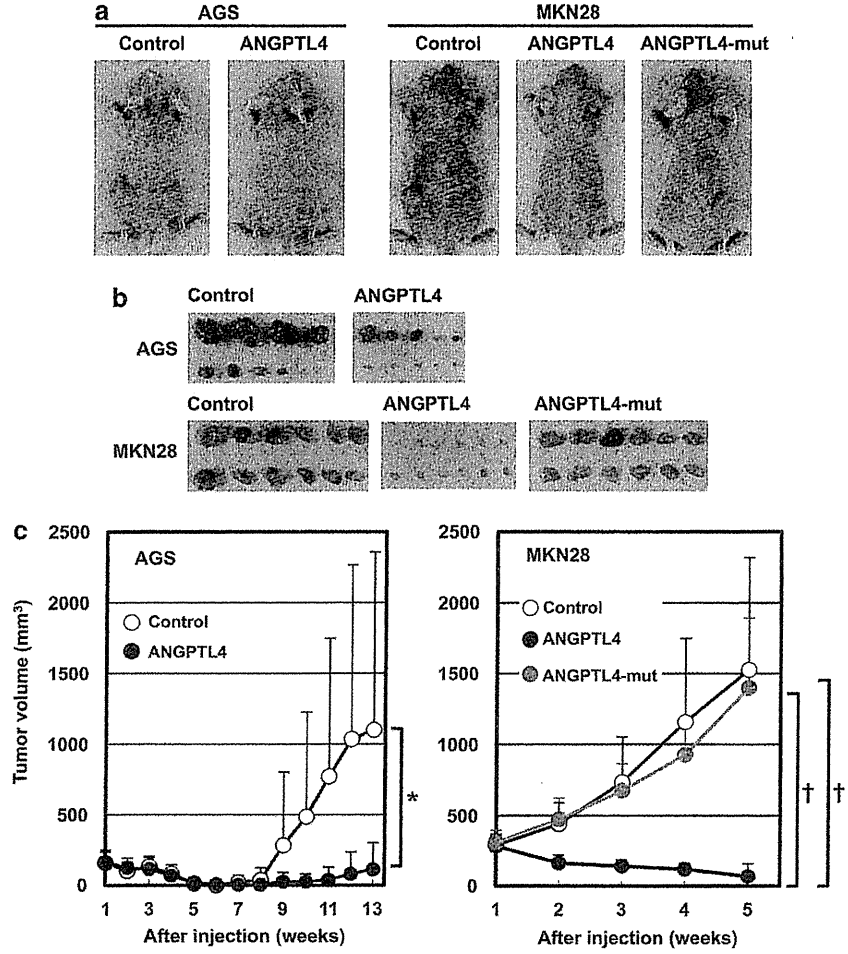

Figure 2. The effect of *ANGPTL4* and its mutant with the 21-bp deletion on tumor formation. The complementary DNA of wild-type *ANGPTL4*, its mutant with the deletion, and *EGFP* as a control were inserted into a mammalian expression vector pIRESpuro3 with the human cytomegalovirus immediate early promoter (Clontech, Mountain View, CA, USA). Individual vectors were transfected into MKN28 or AGS gastric cancer cell lines, and transfectants were selected with puromycin (0.3 μg/ml). Athymic nude mice (BALB/cAJc1-nu/nu, CLEA, Tokyo, Japan) were subcutaneously injected with cells (1×10^7 cells) mixed with an equal volume of Matrigel (BD Biosciences, San Diego, CA, USA). All the animal experiments were approved by the Committee for Ethics in Animal Experimentation, and conducted in accordance with the Guidelines for Animal Experiments of the National Cancer Center. (**a**) Representative photographs of transplanted tumors at 13 weeks (AGS) and 5 weeks (MKN28). *ANGPTL4* markedly suppressed tumor formation, while its mutant with the deletion lacked the activity. (**b**) Macroscopic views of the tumors resected at 13 weeks (AGS) and at 5 weeks (MKN28). Introduction of *ANGPTL4* markedly suppressed tumor sizes in both cell lines. The variable degree of suppression in AGS might have been due to the lower ANGPTL4 expression level (Supplementary Figure S5c). (**c**) Tumor growth curves after the injection. The volume of tumor (mm^3) was calculated by the formula: (length × width^2)/2. A tumor volume is shown as a mean ± s.d. ($N = 10$ in AGS and $N = 12$ in MKN28). $^*P < 0.05$, $^\dagger P < 0.001$ (Student's *t*-test).

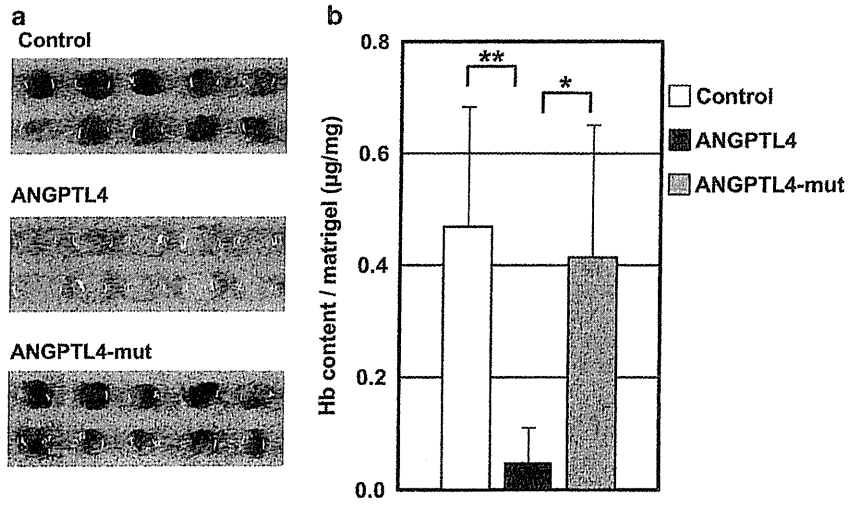

Figure 3. For caption please see page 2276.

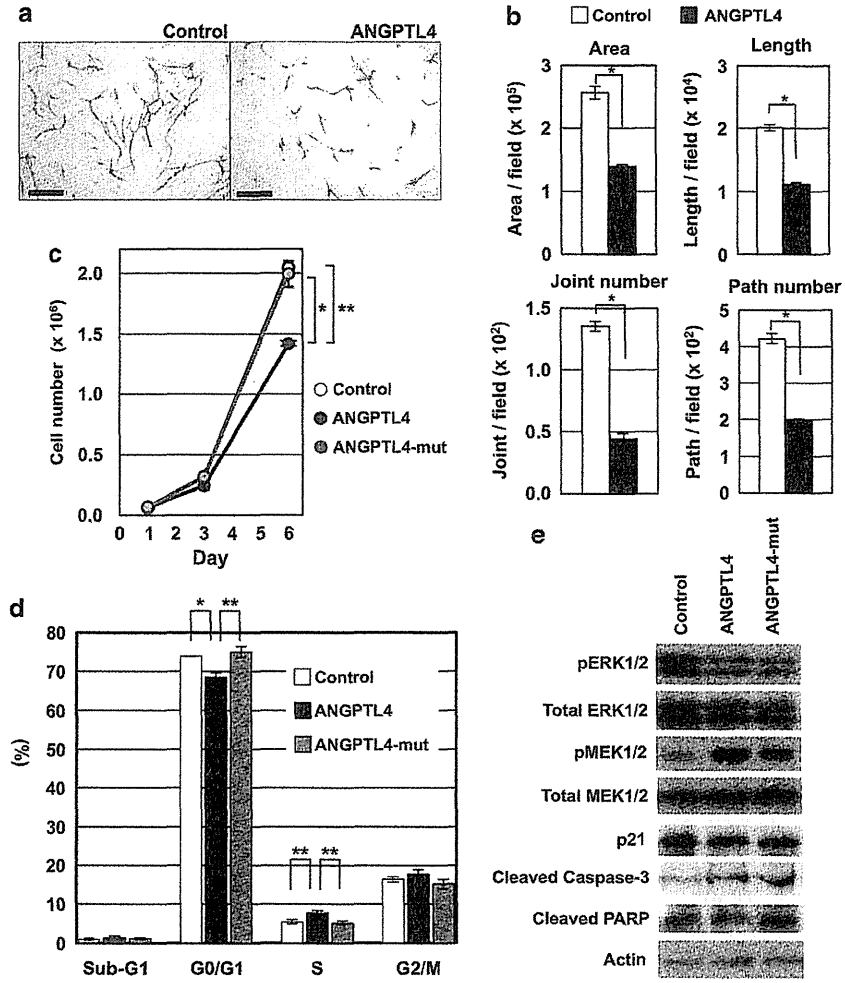

Figure 4. *In vitro* anti-angiogenic activity of tumor-derived ANGPTL4 and its molecular mechanisms. (**a**) Suppression of vascular tube formation by ANGPTL4. A conditioned medium was prepared by mixing the medium of subconfluent MKN28 cells expressing control or *ANGPTL4* and the HUVEC medium with VEGF-A (10 ng/ml) at 1:2. HUVECs on feeder neonatal normal human dermal fibroblast cells (Angiogenesis Kit, Kurabo, Osaka, Japan) arrived from the manufacturer on day 0, and the conditioned medium was supplemented on days 1, 4, 7 and 9. On day 11, cells were fixed and endothelial tubes were stained with anti-CD31antibody (BD Pharmingen, San Diego, CA, USA). The experiment was conducted in triplicate. Scale bars, 50 μm. (**b**) Quantification of the extent of vascular tube formation. Four parameters were scored in nine visual fields per well using the angiogenesis quantification software (Kurabo), and all the four parameters were shown to be suppressed by ANGPTL4. The results are shown as a mean ± s.d. $*P<0.001$ (Student's *t*-test). (**c**) Suppression of the HUVEC growth by ANGPTL4, but not by its mutant with the deletion. HUVECs were seeded at a density of 1×10^5 cells/10-cm dish on day 0, and the conditioned medium prepared as in **a** was supplemented on days 1, 3 and 5. The number of cells was counted on day 3 and day 6 by a Countess Automated Cell Counter (Invitrogen, Carlsbad, CA, USA). Each culture was carried out three times, and the result is shown as a mean ± s.d. $*P=8.4\times10^{-4}$, $**P=5.5\times10^{-5}$ (Student's *t*-test). (**d**) The effects of ANGPTL4 and its mutant with the deletion on the cell cycle of HUVECs. The HUVECs on day 6 of **c** were stained with propidium iodide, and cell populations in different phases of the cell cycle were determined by a FACS Caliber flow cytometer (Becton Dickinson, San Diego, CA). S-phase arrest was observed in HUVECs exposed to ANGPTL4, but not to its mutant with the deletion. $*P<0.05$, $**P<0.01$ (Student's *t*-test). (**e**) Immunoblot analysis of various signal molecules in HUVECs on day 6 of **c**. Decrease of pERK1/2 and increase of pMEK1/2 were induced by ANGPTL4 and also by its mutant with the deletion. This was considered because the deletion mutation affected mainly the interaction between ANGPTL4 and extracellular matrix, which was not necessary for this analysis. Primary antibodies used include anti-phospho-ERK1/2 (1:100, Cell Signaling Technology, Danvers, MA, USA), anti-total ERK1/2 (1:100, Cell Signaling Technology), anti-phospho-MEK1/2 (1:1000, Cell Signaling Technology), anti-total MEK1/2 (1:100, Cell Signaling Technology), anti-p21 (1:200, Cell Signaling Technology), anti-cleaved Caspase-3 (Asp175) (1:200, Cell Signaling Technology), anti-cleaved PARP (Asp214) (1:200, Cell Signaling Technology) and anti-actin (1:1000, Santa Cruz Biotechnology, Santa Cruz, CA, USA). Secondary antibodies conjugated to horseradish peroxidase were obtained from Cell Signaling Technology.

Figure 3. Inhibition of tumor angiogenesis by *ANGPTL4*, but not by its mutant with the deletion. (**a**) Macroscopic view of the Matrigel plugs recovered in the Matrigel plug assay. Matrigel (Matrigel basement membrane matrix high concentration, phenol red-free, BD Biosciences) was mixed with the MKN28 cells (5×10^6 cells) expressing control, *ANGPTL4*, or its mutant with the deletion. The Matrigel plug was subcutaneously injected into 5-week-old female athymic nude mice on day 1, and was recovered on day 10. Marked inhibition of tumor angiogenesis by *ANGPTL4*, but not by its mutant with the deletion, was observed. Brown color shows infiltration of blood vessels into the Matrigel plugs. (**b**) Hemoglobin content in the Matrigel plugs ($N=10$). The plugs were homogenized in red blood cell-lysing buffer (Sigma-Aldrich, St Louis, MO, USA), and the supernatants were measured with Drabkin's reagent (Sigma-Aldrich) to quantify the hemoglobin content in the plug. The content is shown as a mean ± s.d. ($N=10$). $*P=8.0\times10^{-4}$, $**P=1.2\times10^{-4}$ (Student's *t*-test).

demethylated the promoter and restored the *ANGPTL4* expression (Supplementary Figure S4). This showed methylation silencing of *ANGPTL4* in these cell lines.

Marked suppression of *in vivo* tumor growth by ANGPTL4, but not by a mutant with the deletion

The function of ANGPTL4, along with its mutant with the deletion, was examined by stably introducing wild-type or mutant *ANGPTL4* complementary DNA into MKN28 and AGS. The expression levels of the exogenous wild-type *ANGPTL4* and its mutant were kept in the range comparable to its physiological expression in gastric mucosae (Supplementary Figure S5a), and expression of *ANGPTL4* with the deletion mutation was confirmed by the amplification of a shorter size fragment (Supplementary Figure S5b).

Regarding *in vitro* effects, the *ANGPTL4* expression did not affect cell morphology, motility or cell growth (Supplementary Figures S6–S8). However, *in vivo*, sizes of engrafted tumors were strikingly suppressed by the wild-type *ANGPTL4*, markedly in AGS and almost completely in MKN28 (Figure 2). In contrast, when the mutant *ANGPTL4* was expressed in MKN28, it did not show any anti-tumorigenic effect. The presence of ANGPTL4 mRNA and protein expression in the transplanted tumors was confirmed (Supplementary Figures S9 and S10). The role of *ANGPTL4* in tumor development and progression has been highly controversial, but our data clearly showed that *ANGPTL4* suppresses tumor formation, at least in gastric cancers.

Inhibition of tumor angiogenesis as a mechanism for tumor suppression

As a mechanism for tumor suppression by *ANGPTL4*, anti-angiogenic activity of tumor-derived ANGPTL4 was examined. We performed an *in vivo* Matrigel plug angiogenesis assay to observe the vascularization that invades into a Matrigel[31] using MKN28 cells with control (*EGFP*), *ANGPTL4*, and its mutant with the deletion. Ten days after subcutaneous transplantation, the Matrigel plugs containing the control cells showed a high degree of blood vessel recruitment, as visualized by the high content of hemoglobin (Figure 3) and by the staining of CD31-positive vascular endothelial cells (Supplementary Figure S11). In contrast, the Matrigel plugs containing the *ANGPTL4*-expressing cells showed a marked suppression of the blood vessel recruitment. However, *ANGPTL4* with the deletion mutation did not have such activity. The lack of the suppressive effect was in accordance with a report that the CCD was essential for the interaction with the extracellular matrix and for its *in vivo* suppressive activity.[13] These results strongly indicated that the marked anti-angiogenic activity of tumor-derived ANGPTL4 was the cause of the marked suppression of tumor growth by ANGPTL4.

Mechanisms for the anti-angiogenic activity of the tumor-derived ANGPTL4

The mechanisms of how tumor-derived, secreted ANGPTL4 exerts its anti-angiogenic effect were analyzed. First, we conducted a vascular tube formation assay using human umbilical vein endothelial cells (HUVECs). A conditioned medium from *ANGPTL4*-expressing cells suppressed vascular tube formation of HUVECs, as visualized by staining with anti-CD31antibody (Figure 4a), and all the parameters to assess vascular formation were markedly suppressed (Figure 4b). This result showed that a large part of the anti-angiogenic activity of tumor-derived ANGPTL4 was mediated by the suppression of vascular tube formation in the tumor microenvironment.

The effect of the conditioned medium on the growth of HUVECs was then analyzed. The conditioned medium from cells expressing *ANGPTL4*, but not that from cells expressing its mutant with the deletion, suppressed the growth (Figure 4c). Cell cycle analysis showed that the conditioned medium from *ANGPTL4*-expressing cells significantly increased the number of cells in the S phase, suggesting that it induced an S-phase arrest (Figure 4d). However, the amount of p21, a potential inducer of the S-phase arrest,[32] was not increased (Figure 4e). No induction of apoptosis was observed by western blot analysis of apoptosis-related proteins, cleaved Caspase-3 and cleaved PARP (Figure 4e), or by terminal deoxynucleotidyl transferase dUTP nick end labeling (TUNEL) assay (Supplementary Figure S8).

Finally, the effect of tumor-derived ANGPTL4 on the MAPK signaling was analyzed. The conditioned medium from the *ANGPTL4*-expressing cells clearly inhibited the phosphorylation of ERK1/2 (pERK1/2) (Figure 4e), and the phosphorylation of its immediate upstream mediator, pMEK, was in contrast increased. The conditioned medium from the cells expressing the mutant with the deletion showed a similar activity to that of the *ANGPTL4*-expressing cells. As CCD is not important for the delivery to target cells *in vitro* and the fibrinogen-like domain is important for inhibition of the Raf/MEK/ERK signaling,[11] it was considered that the deletion mutation did not affect the inhibition activity.

This study demonstrated that *ANGPTL4* is a mutated and methylation-silenced tumor suppressor whose product is secreted and inhibits angiogenesis. *ANGPTL4* mutation (loss-of-function) was identified for the first time in any type of cancers, and the anti-angiogenic activity of tumor-derived ANGPTL4 was shown here also for the first time. These data warrant further research into utilizing ANGPTL4 as a target of anti-angiogenesis cancer therapy.

CONFLICT OF INTEREST

The authors declare no conflict of interest.

ACKNOWLEDGEMENTS

We are grateful to Dr Masabumi Shibuya, Tokyo Medical and Dental University, for his expert advice. This study was supported by the Third-term Comprehensive Cancer Control Strategy from the Ministry of Health, Labour and Welfare, Japan and by National Cancer Center Research and Development Fund. YN is a recipient of a Research Resident Fellowships from the Foundation for Promotion of Cancer Research.

REFERENCES

1 Knudson AG. Two genetic hits (more or less) to cancer. *Nat Rev Cancer* 2001; **1**: 157–162.
2 Baylin SB, Jones PA. A decade of exploring the cancer epigenome - biological and translational implications. *Nat Rev Cancer* 2011; **11**: 726–734.
3 Kishore R, Losordo DW. Gene therapy for restenosis: biological solution to a biological problem. *J Mol Cell Cardiol* 2007; **42**: 461–468.
4 Lane DP, Cheok CF, Lain S. p53-based cancer therapy. *Cold Spring Harb Perspect Biol* 2010; **2**: a001222.
5 Levine AJ, Oren M. The first 30 years of p53: growing ever more complex. *Nat Rev Cancer* 2009; **9**: 749–758.
6 Suzuki H, Watkins DN, Jair KW, Schuebel KE, Markowitz SD, Chen WD *et al.* Epigenetic inactivation of *SFRP* genes allows constitutive WNT signaling in colorectal cancer. *Nat Genet* 2004; **36**: 417–422.
7 Shi Y, He B, You L, Jablons DM. Roles of secreted frizzled-related proteins in cancer. *Acta Pharmacol Sin* 2007; **28**: 1499–1504.
8 Kaneda A, Kaminishi M, Yanagihara K, Sugimura T, Ushijima T. Identification of silencing of nine genes in human gastric cancers. *Cancer Res* 2002; **62**: 6645–6650.
9 Hattori N, Okochi-Takada E, Kikuyama M, Wakabayashi M, Yamashita S, Ushijima T. Methylation silencing of angiopoietin-like 4 in rat and human mammary carcinomas. *Cancer Sci* 2011; **102**: 1337–1343.
10 Miida T, Hirayama S. Impacts of angiopoietin-like proteins on lipoprotein metabolism and cardiovascular events. *Curr Opin Lipidol* 2010; **21**: 70–75.
11 Yang YH, Wang Y, Lam KS, Yau MH, Cheng KK, Zhang J *et al.* Suppression of the Raf/MEK/ERK signaling cascade and inhibition of angiogenesis by the carboxyl terminus of angiopoietin-like protein 4. *Arterioscler Thromb Vasc Biol* 2008; **28**: 835–840.

12 Ito Y, Oike Y, Yasunaga K, Hamada K, Miyata K, Matsumoto S *et al.* Inhibition of angiogenesis and vascular leakiness by angiopoietin-related protein 4. *Cancer Res* 2003; **63**: 6651–6657.
13 Chomel C, Cazes A, Faye C, Bignon M, Gomez E, Ardidie-Robouant C *et al.* Interaction of the coiled-coil domain with glycosaminoglycans protects angiopoietin-like 4 from proteolysis and regulates its antiangiogenic activity. *FASEB J* 2009; **23**: 940–949.
14 Hermann LM, Pinkerton M, Jennings K, Yang L, Grom A, Sowders D *et al.* Angiopoietin-like-4 is a potential angiogenic mediator in arthritis. *Clin Immunol* 2005; **115**: 93–101.
15 Ma T, Jham BC, Hu J, Friedman ER, Basile JR, Molinolo A *et al.* Viral G protein-coupled receptor up-regulates Angiopoietin-like 4 promoting angiogenesis and vascular permeability in Kaposi's sarcoma. *Proc Natl Acad Sci USA* 2010; **107**: 14363–14368.
16 Li KQ, Li WL, Peng SY, Shi XY, Tang HL, Liu YB. Anti-tumor effect of recombinant retroviral vector-mediated human ANGPTL4 gene transfection. *Chin Med J (Engl)* 2004; **117**: 1364–1369.
17 Galaup A, Cazes A, Le Jan S, Philippe J, Connault E, Le Coz E *et al.* Angiopoietin-like 4 prevents metastasis through inhibition of vascular permeability and tumor cell motility and invasiveness. *Proc Natl Acad Sci USA* 2006; **103**: 18721–18726.
18 Padua D, Zhang XH, Wang Q, Nadal C, Gerald WL, Gomis RR *et al.* TGFbeta primes breast tumors for lung metastasis seeding through angiopoietin-like 4. *Cell* 2008; **133**: 66–77.
19 Zhu P, Tan MJ, Huang RL, Tan CK, Chong HC, Pal M *et al.* Angiopoietin-like 4 protein elevates the prosurvival intracellular O_2^-:H_2O_2 ratio and confers anoikis resistance to tumors. *Cancer Cell* 2011; **19**: 401–415.
20 Nakayama T, Hirakawa H, Shibata K, Abe K, Nagayasu T, Taguchi T. Expression of angiopoietin-like 4 in human gastric cancer: ANGPTL4 promotes venous invasion. *Oncol Rep* 2010; **24**: 599–606.
21 Issa JP. CpG island methylator phenotype in cancer. *Nat Rev Cancer* 2004; **4**: 988–993.
22 Ushijima T. Epigenetic field for cancerization. *J Biochem Mol Biol* 2007; **40**: 142–150.
23 Hato T, Tabata M, Oike Y. The role of angiopoietin-like proteins in angiogenesis and metabolism. *Trends Cardiovasc Med* 2008; **18**: 6–14.
24 Oike Y, Akao M, Kubota Y, Suda T. Angiopoietin-like proteins: potential new targets for metabolic syndrome therapy. *Trends Mol Med* 2005; **11**: 473–479.
25 Ge H, Yang G, Huang L, Motola DL, Pourbahrami T, Li C. Oligomerization and regulated proteolytic processing of angiopoietin-like protein 4. *J Biol Chem* 2004; **279**: 2038–2045.
26 Yin W, Romeo S, Chang S, Grishin NV, Hobbs HH, Cohen JC. Genetic variation in ANGPTL4 provides insights into protein processing and function. *J Biol Chem* 2009; **284**: 13213–13222.
27 Mei R, Galipeau PC, Prass C, Berno A, Ghandour G, Patil N *et al.* Genome-wide detection of allelic imbalance using human SNPs and high-density DNA arrays. *Genome Res* 2000; **10**: 1126–1137.
28 Hoglund M, Gorunova L, Andren-Sandberg A, Dawiskiba S, Mitelman F, Johansson B. Cytogenetic and fluorescence in situ hybridization analyses of chromosome 19 aberrations in pancreatic carcinomas: frequent loss of 19p13.3 and gain of 19q13.1-13.2. *Genes Chromosomes Cancer* 1998; **21**: 8–16.
29 Trojan J, Brieger A, Raedle J, Esteller M, Zeuzem S. 5′-CpG island methylation of the *LKB1/STK11* promoter and allelic loss at chromosome 19p13.3 in sporadic colorectal cancer. *Gut* 2000; **47**: 272–276.
30 Sobottka SB, Haase M, Fitze G, Hahn M, Schackert HK, Schackert G. Frequent loss of heterozygosity at the 19p13.3 locus without *LKB1/STK11* mutations in human carcinoma metastases to the brain. *J Neurooncol* 2000; **49**: 187–195.
31 Tanner JE, Forte A, Panchal C. Nucleosomes bind fibroblast growth factor-2 for increased angiogenesis *in vitro* and *in vivo*. *Mol Cancer Res* 2004; **2**: 281–288.
32 Zhu H, Zhang L, Wu S, Teraishi F, Davis JJ, Jacob D *et al.* Induction of S-phase arrest and p21 overexpression by a small molecule 2[[3-(2,3-dichlorophenoxy) propyl] amino]ethanol in correlation with activation of ERK. *Oncogene* 2004; **23**: 4984–4992.
33 Asada K, Ando T, Niwa T, Nanjo S, Watanabe N, Okochi-Takada E *et al. FHL1* on chromosome X is a single-hit gastrointestinal tumor-suppressor gene and contributes to the formation of an epigenetic field defect. *Oncogene* 2012; **32**: 2140–2149.
34 Ando T, Yoshida T, Enomoto S, Asada K, Tatematsu M, Ichinose M *et al.* DNA methylation of microRNA genes in gastric mucosae of gastric cancer patients: its possible involvement in the formation of epigenetic field defect. *Int J Cancer* 2009; **124**: 2367–2374.
35 Enomoto S, Maekita T, Tsukamoto T, Nakajima T, Nakazawa K, Tatematsu M *et al.* Lack of association between CpG island methylator phenotype in human gastric cancers and methylation in their background non-cancerous gastric mucosae. *Cancer Sci* 2007; **98**: 1853–1861.
36 Ota N, Kawakami K, Okuda T, Takehara A, Hiranuma C, Oyama K *et al.* Prognostic significance of $p16^{INK4a}$ hypermethylation in non-small cell lung cancer is evident by quantitative DNA methylation analysis. *Anticancer Res* 2006; **26**: 3729–3732.

Supplementary Information accompanies this paper on the Oncogene website (http://www.nature.com/onc)

PLOS ONE

Loss of the BRCA1-Interacting Helicase BRIP1 Results in Abnormal Mammary Acinar Morphogenesis

Kazuhiro Daino[1,2]*, Tatsuhiko Imaoka[1,2], Takamitsu Morioka[1,2], Shusuke Tani[1], Daisuke Iizuka[1,3], Mayumi Nishimura[1,2], Yoshiya Shimada[1,2]*

1 Radiobiology for Children's Health Program, Research Center for Radiation Protection, National Institute of Radiological Sciences, Chiba, Japan, **2** Radiation Effect Accumulation and Prevention Project, Fukushima Project Headquarters, National Institute of Radiological Sciences, Chiba, Japan, **3** Department of Experimental Oncology, Division of Genome Biology, Research Institute for Radiation Biology and Medicine, Hiroshima University, Hiroshima, Japan

Abstract

BRIP1 is a DNA helicase that directly interacts with the C-terminal BRCT repeat of the breast cancer susceptibility protein BRCA1 and plays an important role in BRCA1-dependent DNA repair and DNA damage–induced checkpoint control. Recent studies implicate *BRIP1* as a moderate/low-penetrance breast cancer susceptibility gene. However, the phenotypic effects of BRIP1 dysfunction and its role in breast cancer tumorigenesis remain unclear. To explore the function of BRIP1 in acinar morphogenesis of mammary epithelial cells, we generated BRIP1-knockdown MCF-10A cells by short hairpin RNA (shRNA)-mediated RNA interference and examined its effect in a three-dimensional culture model. Genome-wide gene expression profiling by microarray and quantitative RT-PCR were performed to identify alterations in gene expression in *BRIP1*-knockdown cells compared with control cells. The microarray data were further investigated using the pathway analysis and Gene Set Enrichment Analysis (GSEA) for pathway identification. *BRIP1* knockdown in non-malignant MCF-10A mammary epithelial cells by RNA interference induced neoplastic-like changes such as abnormal cell adhesion, increased cell proliferation, large and irregular-shaped acini, invasive growth, and defective lumen formation. Differentially expressed genes, including *MCAM*, *COL8A1*, *WIPF1*, *RICH2*, *PCSK5*, *GAS1*, *SATB1*, and *ELF3*, in *BRIP1*-knockdown cells compared with control cells were categorized into several functional groups, such as cell adhesion, polarity, growth, signal transduction, and developmental process. Signaling-pathway analyses showed dysregulation of multiple cellular signaling pathways, involving LPA receptor, Myc, Wnt, PI3K, PTEN as well as DNA damage response, in *BRIP1*-knockdown cells. Loss of BRIP1 thus disrupts normal mammary morphogenesis and causes neoplastic-like changes, possibly via dysregulating multiple cellular signaling pathways functioning in the normal development of mammary glands.

Citation: Daino K, Imaoka T, Morioka T, Tani S, Iizuka D, et al. (2013) Loss of the BRCA1-Interacting Helicase BRIP1 Results in Abnormal Mammary Acinar Morphogenesis. PLoS ONE 8(9): e74013. doi:10.1371/journal.pone.0074013

Editor: Toru Ouchi, University of Chicago, United States of America

Received April 25, 2013; **Accepted** July 25, 2013; **Published** September 6, 2013

Funding: A part of this study was financially supported by a Grant-in-Aid for Young Scientists (B) (#23710075) from the Japan Society for the Promotion of Science. The funder had no role in study design, data collection and analysis, decision to publish, or preparation of the manuscript. No additional external funding was received for this study.

Competing Interests: The authors have declared that no competing interests exist.

* E-mail: k_daino@nirs.go.jp (KD); y_shimad@nirs.go.jp (YS)

Introduction

Breast cancer is one of the most common epithelial malignancies among woman worldwide. Approximately one in ten women will develop breast cancer during their lifetime in industrialized countries. Although the majority of breast cancers are sporadic in origin, an appreciable fraction is caused by inherited predisposition. Germline mutations in the two major susceptibility genes for breast cancer, namely *BRCA1* and *BRCA2*, confer a 60–85% lifetime risk of breast cancer but account for only about 20% of familial breast cancer cases [1–7]. To date, several other breast cancer susceptibility genes, which show low-to-moderate penetrance, have been identified. BRIP1 is one of these genes and truncating mutations confer a 2-fold increase in breast cancer risk [8], [9].

BRIP1 (also known as BACH1 and FANCJ) is a DNA helicase that interacts directly with the breast cancer susceptibility protein BRCA1. BRIP1 plays an important role in controlling BRCA1-dependent DNA repair, DNA damage–induced G2-M checkpoint control, and possibly tumor suppression [10–14]. *BRIP1* gene is located on chromosome 17q22, just distal to the *BRCA1* gene located at 17q21, a region that shows frequent loss of heterozygosity in breast cancers [15], [16]. Several loss-of-function mutations in *BRIP1* gene have been reported in breast cancers and also in the cancer-prone disease Fanconi anemia [17]. In addition, some of mutated BRIP1 proteins has been shown to be unstable, with reduced expression [10], [18]. However, the role of BRIP1 in tumorigenesis of mammary epithelial cells remains unclear.

Phenotypic analysis of mice that have a genetic defect in DNA double-strand break repair shows various developmental abnormalities as well as increased tumorigenesis, suggesting a strong link among DNA damage repair, development, and tumorigenesis [19], [20]. For instance, conditional *BRCA1*-knockout mice display incomplete and abnormal mammary gland development [21]. *BRCA1*-knockdown in human mammary epithelial cells abrogates the ability of the cells to form acini in three-dimensional (3D) culture, suggesting a possible role for BRCA1 in mammary cell differentiation [22]. This developmental process is shown to be mediated by the C-

terminal BRCT repeat of BRCA1, which interacts with several proteins, including BRIP1. This suggests that BRIP1 plays a role in mammary gland development and tumorigenesis in a BRCA1-dependent or independent manner.

Using 3D basement membrane culture of human non-malignant mammary epithelial MCF-10A cells, we have investigated the roles for BRIP1 in mammary gland development and tumorigenesis. We here show for the first time that *BRIP1* knockdown by RNA interference promotes cell proliferation and disrupts acinar architecture, which may result from dysregulation of genes known to be involved in cell adhesion, polarity, growth, signal transduction, and developmental process, and signaling pathways such as LPA, Myc, Wnt, PI3K, and PTEN. In summary, loss of BRIP1 affects multiple cellular signaling pathways, which are known to be critical for normal development of mammary glands, and its dysfunction disrupts acinar formation.

Materials and Methods

Cell Culture and *BRIP1* Knockdown by Lentiviral Transduction of shRNA

MCF-10A cells obtained from American Type Culture Collection, were maintained in a 1:1 mix of Dulbecco's modified Eagle's (DME) and Ham's F12 media supplemented with 5% equine serum, 10 μg/ml bovine insulin, 20 ng/ml epidermal growth factor, 100 ng/ml cholera toxin, and 0.5 μg/ml hydrocortisone as described [23]. Lentiviral transduction of MCF-10A cells with particles for shRNAs targeting BRIP1 (SHCLNV-NM_032043, MISSION shRNA; Sigma-Aldrich), or scrambled non-target negative control (SHC002V) was performed according to the manufacturer's protocol. The transduced MCF-10A cells were selected with 1 μg/ml puromycin. The shRNA that showed the highest knockdown efficiency among 5 designed sequences compared with the non-target control was selected.

Western Blot Analysis

Cellular proteins were extracted with Cell Lysis Buffer (Cell Signaling Technology) containing 1 mM phenylmethylsulfonyl fluoride. Equal amounts of protein were fractionated by 7% SDS-PAGE, transferred to a polyvinylidene difluoride membrane, and reacted with antibodies against BRIP1 (B1310; Sigma-Aldrich), and β-actin (AC-74; Sigma-Aldrich). The protein bands were visualized by enhanced chemiluminescence using ECL Plus Western Blotting Detection System (GE Healthcare).

3D Morphogenesis Assays

Cells were cultured on top of a polymerized layer of 100% Matrigel in a 1:1 mix of DME and Ham's F12 media supplemented with 2% equine serum, 10 μg/ml insulin, 5 ng/ml epidermal growth factor, 100 ng/ml cholera toxin, 0.5 μg/ml hydrocortisone, and 2% reconstituted basement membrane (Matrigel; BD Biosciences) in a four- or eight-well chamber slide as described [23]. Cells were seeded as single cells at low density of 2.5×10^3 cells per 0.7 cm^2 well. At this low initial cell density, individual cells were not in contact under the microscope, and therefore, a possible contribution of cell aggregation to form larger acini structures is excluded. For the acinar structure size calculations, the sizes of at least 150 distinct structures were measured on photomicrographs using ImageJ software (http://rsb.info.nih.gov/ij/). After fixing cells with formalin, slides were mounted with Vectashield mounting medium containing 4′,6-diamidino-2-phenylindole (DAPI; Vector Laboratories) for nuclear staining. Images were acquired with an all-in-one fluorescence microscope (Biozero BZ-8000; Keyence, Osaka, Japan) and analyzed with BZ-Analyzer (Keyence).

Histology and Immunohistochemistry

Paraffin-embedded/formalin-fixed sections (4 μm thick) of the acini were stained with hematoxylin and eosin or antibody to Ki-67 (clone 7B11; Invitrogen). Antigen–antibody complexes were detected using an anti-mouse secondary antibody and an avidin-biotin complex system (Vector Laboratories) using 3,3′-diaminobenzidine as the chromogen. The percentage of Ki-67-positive cells was determined by counting cells of at least 100 distinct acini in the section.

DNA Microarray Analysis

Samples were harvested from three different clones of non-target and *BRIP1* shRNA-transduced cells at three time points, 4, 8, and 12 days, after cell seeding in Matrigel. Total RNA was extracted, labeled with Cyanine 3-CTP, and hybridized with human oligonucleotide microarrays (whole-human genome microarray; Agilent Technologies) as described [24]. The raw microarray data were normalized and analyzed using GeneSpring GX 11.5.1 software (Agilent Technologies). Expression data for selected genes were visualized using TIGR MultiExperiment Viewer software (available at http://www.tm4.org/mev.html). The microarray data have been deposited in the Gene Expression Omnibus database (www.ncbi.nlm.nih.gov/geo) under accession number GSE33218. Microarray data were analyzed using GSEA v2.0 [25], [26]. Detailed information is provided in Methods S1.

Quantitative RT-PCR

Total RNA was isolated from exponentially growing cells in Petri dishes and from 3D cultured cells using the RNeasy kit (Qiagen). First-strand cDNA was synthesized from total RNA as described (Ishida et al., 2010) [24]. The PCR reaction was performed on the Mx3000P real-time PCR system (Stratagene, La Jolla, CA). Primer sequence information is available in Table S5.

Statistical Analysis

Statistical analysis was carried out with GraphPad StatMate software version 3.0 (ATMS, Tokyo, Japan). Comparison between two groups was done using Student's *t*-test or non-parametric Mann–Whitney *U*-test. $P<0.05$ was considered to be statistically significant.

Tumor Growth in Nude Mice

All animal studies were approved by the Institutional Animal Care and Use Committee of the National Institute of Radiological Sciences. 5×10^6 cells from two different clones of non-target shRNA-transduced cells, three different clones of *BRIP1* shRNA-transduced cells, MCF-7 and MDA-MB-231 human breast cancer cells, as positive controls, were resuspended in 25 μl of phosphate-buffered saline (PBS), mixed with 25 μl of Matrigel, and injected into bilateral abdominal fat pads containing mammary glands of 6-week-old female nude mice (BALB/cAJcl-nu/nu; Clea Japan, Tokyo, Japan; n = 20) under isoflurane anesthesia, and monitored for 10 weeks. Mice were then killed by exsanguination under isoflurane anesthesia and autopsied. Abdominal fat pads were extended on glass slides and fixed in 10% buffered formalin. Hematoxylin-stained whole-mount preparations were observed under a dissection microscope for the occurence of tumors.

Results

Generation of BRIP1-knockdown Mammary Epithelial Cells

To explore the function of BRIP1 in acinar morphogenesis of mammary epithelial cells, we generated stable *BRIP1*-knockdown clones by shRNA vector transduction into MCF-10A human non-malignant mammary epithelial cells. *BRIP1* knockdown was confirmed by western blotting (Fig. 1A). In conventional 2D culture, *BRIP1*-knockdown cells formed loose sheets with rounded and loosely attached cells, suggesting weak cellular adherence (Fig. S1).

Loss of BRIP1 Causes Abnormal Acinar Morphogenesis

To determine whether *BRIP1* knockdown affects the formation of polarized spherical acini, mammary epithelial cells were grown and monitored in 3D culture. We observed that the acini formed by *BRIP1*-knockdown cells were significantly larger than the control acini after 4 days of culture (Fig. 1B and C). Additionally, *BRIP1*-knockdown cells formed irregular-shaped acinar structures after 8 days of culture (Fig. 1B). In 20 days, the control cells developed into organized acini with hollow lumens (Fig. 2C and D). In contrast, the *BRIP1*-knockdown cells formed large irregular-shaped aggregates with filled lumens and were also characterized by increased cell size, filopodia formation, loss of cellular polarity, nuclear atypia, and nuclear stratification (Fig. 2A, B, E and F). *BRIP1*-knockdown cells also had a 3-fold higher rate of

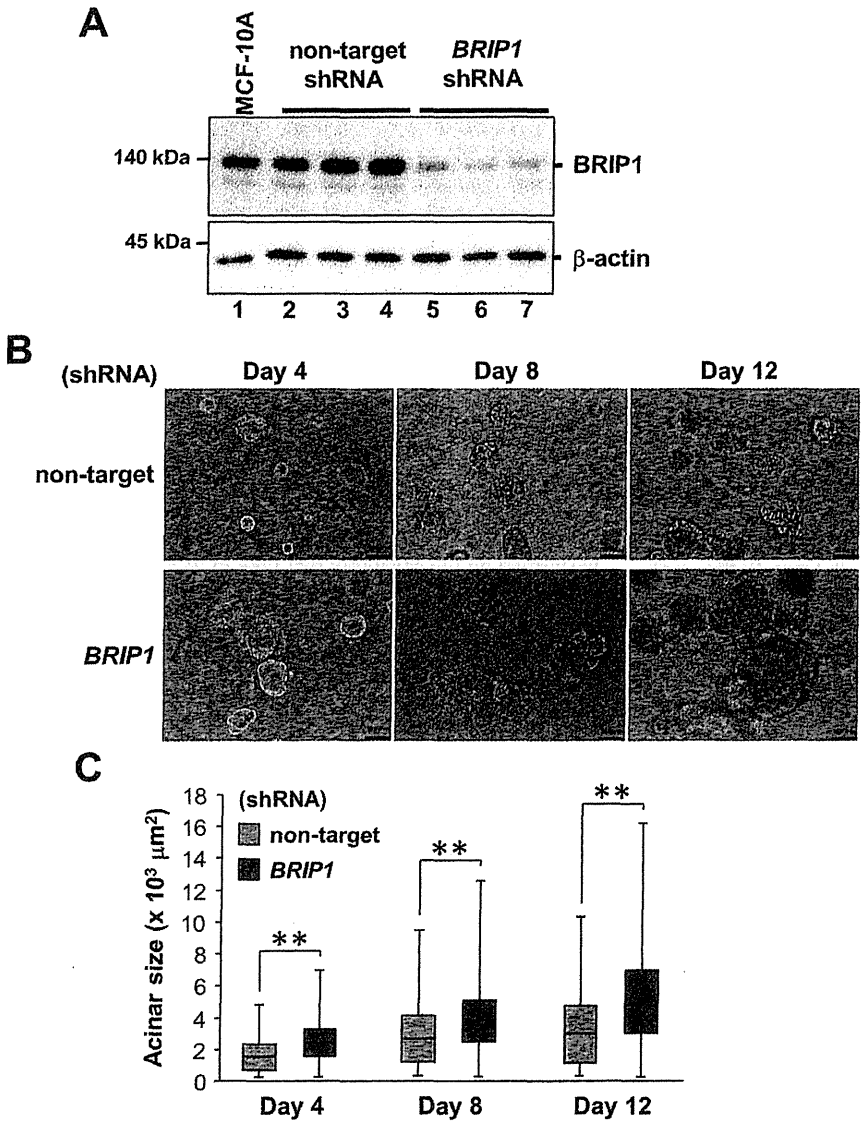

Figure 1. *BRIP1* knockdown in mammary epithelial cells impairs acinus formation. (**A**) *BRIP1* knockdown by lentiviral-mediated delivery of shRNA. Expression of BRIP1 protein in the parental MCF-10A cells (lane 1), three different clones of non-target (lanes 2–4), and *BRIP1* shRNA-transduced (lanes 5–7) cells was analyzed by western blotting with anti-BRIP1. β-actin was used as a loading control. (**B**) Phase-contrast images of cells transduced with non-target shRNA or *BRIP1*-specific shRNA in 3D culture at days 4, 8, and 12. Scale bars, 50 μm. (**C**) Quantification of the size of the acinar structure of the cell lines in 3D culture at days 4, 8, and 12. The median values are indicated with horizontal bars in the boxes. The boxes contain the values between the 25th and 75th percentiles. The whiskers extend to the maximum and minimum values. Comparison between two groups was done using the non-parametric Mann–Whitney *U*-test. $^{**}P<0.001$.
doi:10.1371/journal.pone.0074013.g001

proliferation fraction than the control cells as assessed by Ki-67 immunohistochemistry, even after the control cells formed growth-arrested acini by day 20 (Fig. 2G). These observations suggested that BRIP1 plays a key role in maintaining acinar architecture and that loss of BRIP1 induces a neoplastic-like phenotype in mammary epithelial cells.

Loss of BRIP1 Induces Dysregulation of Multiple Cellular Signaling Pathways

To reveal the genes affected by the loss of BRIP1 during acinar morphogenesis, we performed microarray analysis to clarify the genes differentially expressed during acinar morphogenesis of *BRIP1*-knockdown cells comparing with control cells. Principal component analysis showed that the gene expression profile in the *BRIP1*-knockdown cells during acinar morphogenesis was distinct from that of control cells (Fig. S2A). We identified 379, 288, and 314 transcripts, which were differentially expressed (≥2-fold difference) in 3D culture of *BRIP1*-knockdown cells compared with control cells at 4, 8, and 12 days after culture, respectively (Tables S1–3). Gene Ontology (GO) analysis revealed that subsets of the differentially expressed genes were involved in signal transduction, metabolic processes, developmental process, and cell adhesion, suggesting a link between DNA damage repair and morphogenetic process (Fig. S2B). We also identified 88 transcripts that were consistently up- or down-regulated (fold change ≥2) throughout acinar morphogenesis (Fig. 3A). Table 1 lists selected differentially expressed genes (fold change ≥5). Among them, *SATB1*, which is regarded as a key transcriptional regulator in breast cancer development and metastasis [27], showed high-level expression in *BRIP1*-knockdown cells compared with control cells. We selected several other tumor-associated genes, namely *RICH2*, *PCSK5*, *ELF3*, *WIPF1*, *MCAM*, *COL8A1*, and *GAS1*, based on a literature search, and the changes in gene expression were validated by quantitative real-time reverse transcription-PCR (RT-PCR) (Fig. 3B). Signaling-pathway analysis of the differentially expressed genes revealed enrichment for pathways such as lysophosphatidic acid (LPA) receptor signaling, and oxygen homeostasis, followed by telomerase regulation, Myc signaling and Wnt signaling (Fig. 3C). To further explore the microarray data, gene set enrichment analysis (GSEA) was used to identify groups of functionally related genes for their degree of global up- or down-regulation following *BRIP1* knockdown. This approach identified 33 gene sets that were significantly correlated with *BRIP1* knockdown (Table S4). As shown in Fig. 3D, the gene sets that correlated positively with *BRIP1* knockdown included signaling pathways involved in DNA damage response and cell proliferation, such as ATM, p53 and phosphatidylinositol pathways. In contrast, the negatively correlated gene sets included phosphatase and tensin homologue deleted from chromosome 10 (PTEN) and several cellular metabolic pathways (Fig. 3D and Table S4).

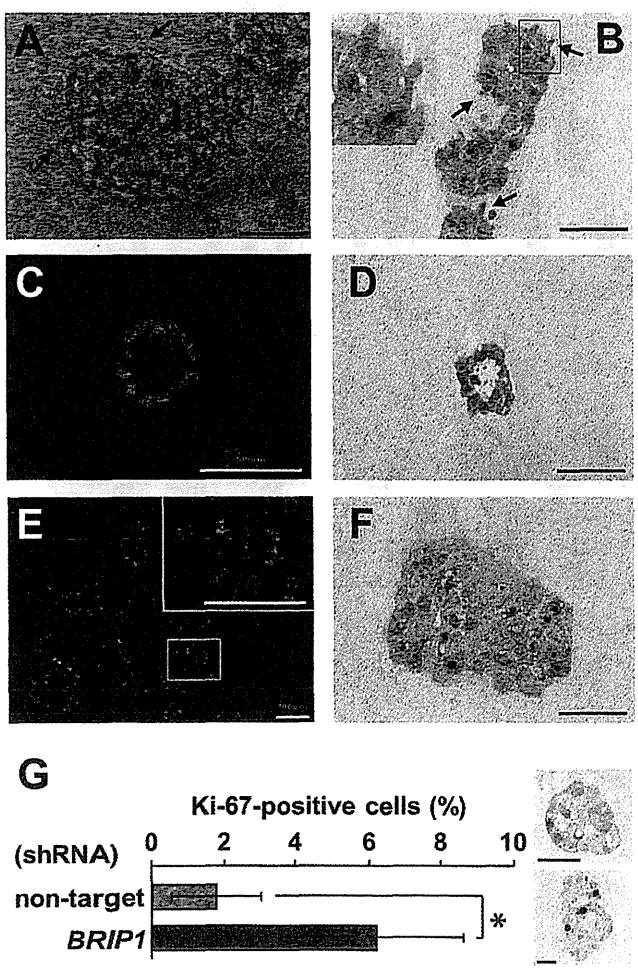

Figure 2. *BRIP1* knockdown induces neoplastic-like changes in mammary acini. Phase-contrast image (**A**) and hematoxylin and eosin-stained section (**B**) of the *BRIP1* shRNA–transduced cells in 3D culture at day 17. Arrows indicate cells with filopodia. The boxed area is enlarged in the inset (**B**). DAPI-stained nuclei (**C, E**) and hematoxylin and eosin-stained section (**D, F**) of cells transduced with the non-target shRNA (**C, D**) or *BRIP1*-specific shRNA (**E, F**) after 20 days in 3D culture. The area indicated by the box is enlarged in the inset (**E**). Scale bars, 50 μm. (**G**) Ki-67 immunostaining of cells transduced with non-target shRNA or *BRIP1*-specific shRNA in 3D culture at day 20. Representative image of Ki-67-stained section of acinar cells transduced with non-target shRNA (*upper right*) or BRIP1-specific shRNA (*lower right*) was shown. Scale bars, 50 μm. Error bars represent the ± SD of the means determined from two independent experiments. Statistical significance was calculated using the Student's t-test. *$P<0.01$.
doi:10.1371/journal.pone.0074013.g002

Tumor Growth in Nude Mice

To determine whether the *BRIP1*-knockdown cells become tumorigenic, we injected two different clones of non-target shRNA-transduced cells and three different clones of *BRIP1* shRNA-transduced cells into both sides of the mammary fat pads of 6-week-old female nude mice (5×10^6 cells on each side at 6 sites for each non-target shRNA-transduced clones and 6 to 8 sites for each *BRIP1* shRNA-transduced clones), and observed for 10 weeks. The *BRIP1*-knockdown cells did not induce tumor formation in nude mice. In this study, we also transplanted MCF-7 and MDA-MB-231 human breast cancer cells into the mammary fat pad as positive controls and these cells did form tumors (data not shown). These results indicate that loss of BRIP1 alone is insufficient to induce tumor formation.

Discussion

The development of mammary epithelial acini follows a series of morphogenetic processes, including cell migration, cell-cell communication, epithelial polarity establishment, differentiation, and hollow lumen formation by luminal cell death [23]. Here, we revealed that the BRCA1-interacting helicase BRIP1 has important roles in promoting normal acinar morphogenesis and loss of BRIP1 disrupts acinar formation possibly through the dysregulation of multiple celluler signaling pathways.

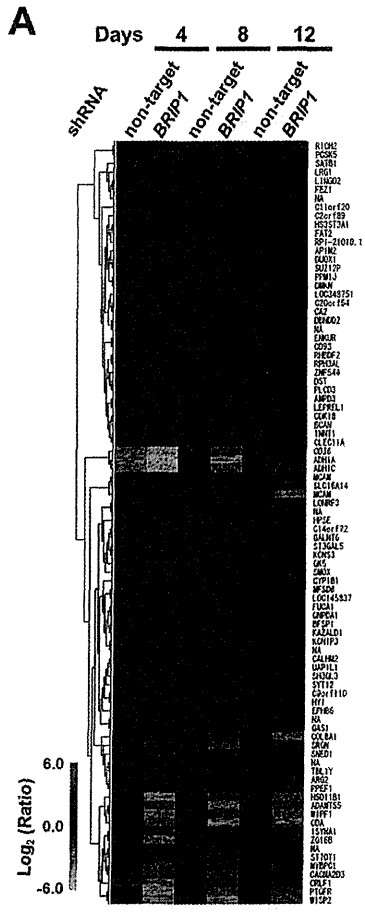

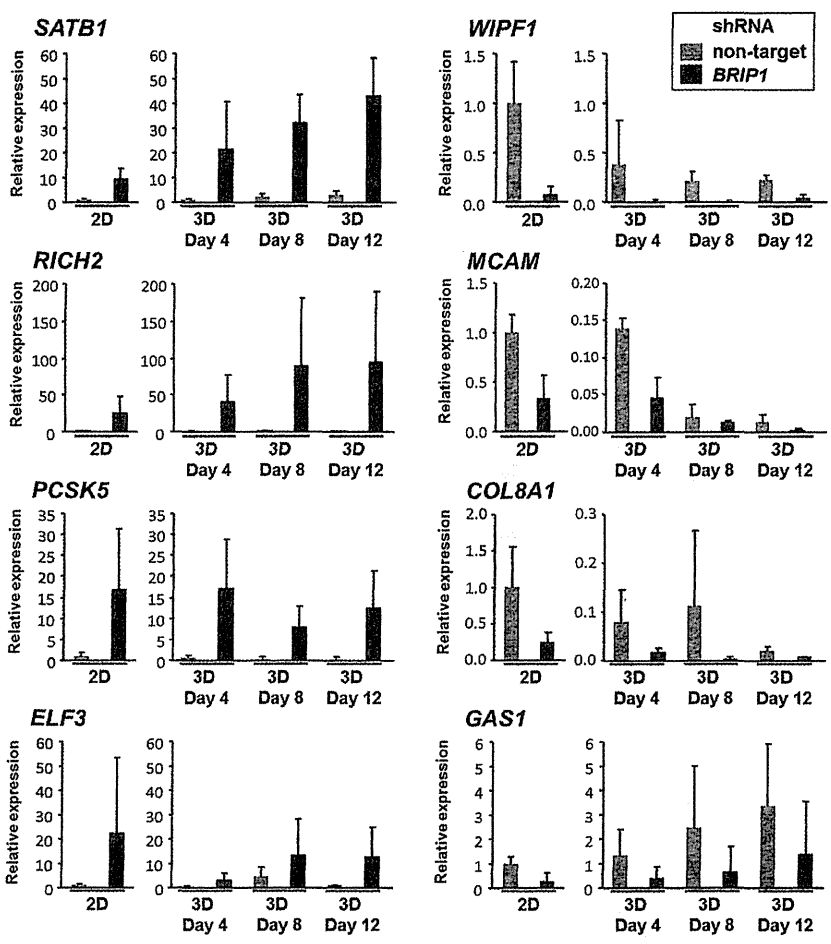

C

Significant signaling pathway (*P*-value)	Genes
Day 4	
· **LPA receptor mediated events** (*0.019*)	*ERC1, LPAR2,* ***GNAS****, LCK, TIAM1, TRIP6, PRKD1, AKT1*
· **Hypoxic and oxygen homeostasis regulation of HIF1-α** (*0.040*)	***CXCL12, HIF3A****, ID2, TP53,* ***TFF3, SERPINB2****, AKT1,* ***HDAC9, MIA3, TIMP1****, GATA2, PFKFB3, HK2*
Day 8	
· **Regulation of telomerase** (*0.015*)	*NCL, MYC, ACD, PTGES3, SP1, NR2F2*
· **Validated target of Myc transcriptional activation** (*0.024*)	*ELF4A1, PDCD10, PFKM, HSPD1, GAPDH, PTMA, NCL, BMI1*
· **Myc pathway** (*0.032*)	*CREB1, EIF4A1, MYC, PTMA, HSPD1, PDCD10, PFKM,* ***GADD45A****, NCL, GAPDH, BMI1,* ***PDGFRB****, SP1*
Day 12	
· **Regulation of Wnt-mediated β-catenin signaling and target gene transcription** (*0.020*)	***CTDSP2****, RNF4, FKBP4,* ***PA2G4, MYC****, SMARCA4,* ***HNRNPA1****, HBP1, AXIN2, CTDSP1,* ***DKK1****, TNIK, AES, MAK,* ***TCF4****, PIAS1, LATS2, KLK3,* ***SP5***
· **Effects of botulinum toxin** (*0.022*)	***STX1A****, STXBP1, RAB3GAP2*
· **Coregulation of androgen receptor activity** (*0.032*)	***PA2G4****, FKBP4,* ***HNRNPA1****, RNF4, PIAS1,* ***CTDSP2****, LATS2, KLK3, CTDSP1, MAK,* ***TCF4***
· **Wnt signaling network** (*0.046*)	***MYC****, SMARCA4,* ***CTDSP2****, RNF4,* ***CHD7****, FKBP4,* ***PA2G4****,* ***HNRNPA1****, AXIN2, PIP4K2A, LATS2, PIAS1, PIP5K1B,* ***TCF4****, LRP6, AES, CTDSP1, TNIK, MAK, KLK3,* ***SP5****,* ***DKK1****, HBP1*

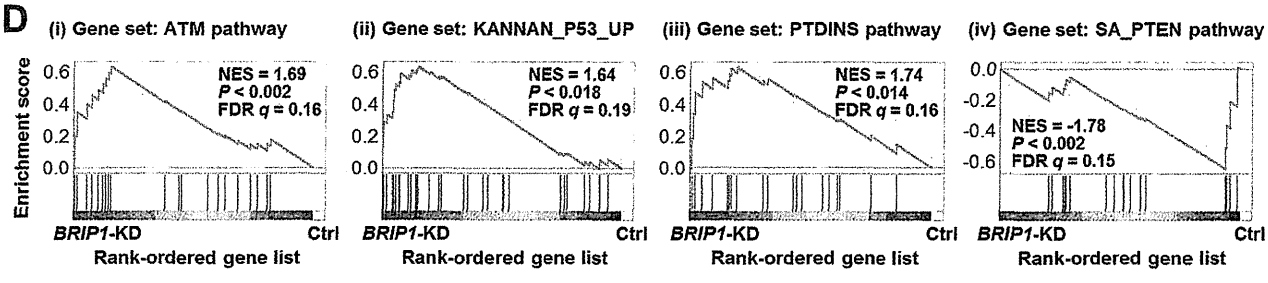

Figure 3. Differentially expressed genes during acinar morphogenesis of *BRIP1*-knockdown mammary epithelial cells. (**A**) Heat map representing the different expression changes of 88 transcripts in *BRIP1* shRNA–transduced cells during acinar morphogenesis compared with non-target shRNA–transduced cells ($P<0.05$; ≥2-fold change). (**B**) Quantitative RT-PCR validation of selected gene expression changes in *BRIP1*-knockdown cells during acinar morphogenesis. The data shown are the mean ± SD of at least two independent experiments with three different clones of shRNA–transduced cells. (**C**) Significantly enriched genes in signaling pathways in the *BRIP1*-knockdown cells during acinar morphogenesis ($P<0.05$). Up- or down-regulated genes are shown in red or blue, respectively. Genes exhibiting a ≥2-fold change in the *BRIP1* shRNA–transduced cells compared with non-target shRNA–transduced cells are indicated in bold. (**D**) GSEA of gene sets up- or down-regulated in 3D-cultured *BRIP1*-knockdown cells compared with control cells. Gene sets from the C2 collection of the Molecular Signatures Database were tested for enrichment in the list of genes ranked by expression change in *BRIP1*-knockdown cells versus control cells. Representative GSEA plots of the enriched gene sets are displayed ($P<0.05$ and FDR $q<0.25$). NES, normalized enrichment score; FDR, false discovery rate; KD, knockdown; Ctrl, control; PTDINS, phosphatidylinositol.
doi:10.1371/journal.pone.0074013.g003

Our microarray analysis revealed abnormalities in the expression of multiple genes in several signaling pathways in *BRIP1*-knockdown cells (Fig. 3). Alterations in components of the LPA, Myc, Wnt signaling pathways have been implicated in breast cancer development. LPA has a variety of biological actions in cell proliferation, survival, motility, and invasion [28], [29]. Up-regulation of LPA receptors are observed in breast cancer and activation of MAPK and phosphatidylinositol 3-kinase (PI3K)/AKT pathways by LPA are implicated in breast cancer development and progression [30], [31]. Myc is a downstream target of multiple signaling pathways, including MAPK and Wnt, and functions as a transcription factor that regulates numerous genes involved in cell growth, transformation, and angiogenesis. An abnormality in the Myc-regulated pathway is frequently reported in breast cancer [32]. Interestingly, loss of BRCA1 accompanied with Myc over-expression accelerates breast cancer development, especially basal-like breast cancer [33]. Wnt signals play a critical role in regulating several stages of mammary gland growth and differentiation, and dysregulation of Wnt signaling causes breast cancer [34]. In addition, GSEA of *BRIP1*-knockdown cells indicated a significant increase in the expression of genes related to the ATM, p53, and phosphatidylinositol signaling pathways as well as a decrease in the expression of genes involved in PTEN signaling pathway. Activation of the DNA-

Table 1. Dysregulated genes in *BRIP1*-knockdown cells during acinar morphogenesis (ANOVA, $P<0.05$; fold change ≥5.0).

Gene symbol	Name	GenBank ID	Fold change*		
			4d	8d	12d
PCSK5	Proprotein convertase subtilisin/kexin type 5	NM_006200	54.3	25.8	22.7
RICH2	Rho-type GTPase-activating protein RICH2	NM_014859	17.2	64.5	44.3
SATB1	SATB homeobox 1, transcript variant 1	NM_002971	12.9	8.8	9.1
LINGO2	Leucine rich repeat and Ig domain containing 2	NM_152570	7.9	7.4	7.4
FEZ1	Fasciculation and elongation protein zeta 1 (zygin I), transcript variant 1	NM_005103	7.4	7.6	5.3
none	cDNA FLJ61137 complete cds, highly similar to Zinc finger protein 302	AK297551	6.2	4.8	4.2
C11orf20	Chromosome 11 open reading frame 20	NM_001039496	6.0	2.6	1.9
LRG1	Leucine-rich alpha-2-glycoprotein 1	NM_052972	2.8	5.3	4.9
CACNA2D3	Calcium channel alpha2-delta3 subunit	AJ272268	−2.0	−5.3	−4.7
CRLF1	Cytokine receptor-like factor 1	NM_004750	−2.2	−4.2	−6.0
CD36	CD36 molecule (thrombospondin receptor), transcript variant 2	NM_001001547	−2.4	−5.1	−3.9
MCAM	Melanoma cell adhesion molecule	NM_006500	−3.0	−2.2	−5.0
ADH1C	Alcohol dehydrogenase 1C (class I), gamma polypeptide	NM_000669	−3.0	−5.7	−6.6
WISP2	WNT1 inducible signaling pathway protein 2	NM_003881	−3.2	−8.1	−11.5
ISYNA1	Inositol-3-phosphate synthase 1, transcript variant 1	NM_016368	−3.2	−6.7	−3.3
ADH1A	Alcohol dehydrogenase 1A (class I), alpha polypeptide	NM_000667	−3.9	−10.6	−5.5
SRGN	Serglycin	NM_002727	−5.2	−4.0	−2.8
COL8A1	Collagen, type VIII, alpha 1, transcript variant 1	NM_001850	−5.8	−8.6	−4.1
SNED1	Sushi, nidogen and EGF-like domains 1	NM_001080437	−6.0	−2.8	−1.7
COL8A1	Collagen, type VIII, alpha 1	AL359062	−6.4	−9.7	−7.7
PTGFR	Prostaglandin F receptor (FP), transcript variant 2	NM_001039585	−8.3	−4.6	−7.0
CDA	Cytidine deaminase	NM_001785	−8.8	−11.0	−8.1
ADAMTS5	ADAM metallopeptidase with thrombospondin type 1 motif, 5	NM_007038	−9.2	−10.0	−6.3
WIPF1	WAS/WASL interacting protein family, member 1, transcript variant 2	NM_001077269	−10.2	−6.3	−8.0
HSD11B1	Hydroxysteroid (11-beta) dehydrogenase 1, transcript variant 2	NM_181755	−11.9	−6.8	−3.6

*A positive fold change indicates increased expression in the *BRIP1*-knockdown cells, and a negative fold change indicates decreased expression in the cells compared with control cells.
doi:10.1371/journal.pone.0074013.t001

damage response mediated by the ATM-p53 pathway in *BRIP1*-knockdown cells is consistent with a role of BRIP1 in maintaining genomic stability [35], and activation of the ATM-p53 pathway is also linked to genomic instability in precancerous cells [36–38]. On the other hand, reduced expression of the tumor suppressor PTEN correlates with breast cancer progression [39]. Down-regulation of genes associated with PTEN signaling and up-regulation of phosphatidylinositol signaling in *BRIP1*-knockdown cells are consistent with PTEN's role as a negative regulator of phosphatidylinositol 3-kinase (PI3K) activity. In fact, abnormalities in *PTEN* or *PI3K* expression induce hyperproliferation of epithelial cells and disruption of cell polarity [40–42]. Thus, BRIP1 may function as tumor suppressor by affecting these tumor suppressive signaling pathways in the mammary glands.

Notably, transcriptional regulator *SATB1*, Rho-type GTPase-activating protein RICH2 and pro-protein convertase PCSK5 were over-expressed in *BRIP1*-knockdown cells (Table 1 and Fig. 3B). SATB1 is reportedly up-regulated in aggressive breast cancer and is proposed to reprogram the global expression profile of multiple genes involved in cell adhesion, polarity, and growth, as well as the above-mentioned phosphatidylinositol signaling [27], [43]. Ectopic expression of SATB1 is shown to induce tumor-like morphology in 3D culture and lead to tumor formation and lung metastasis in nude mice [44]. RICH2 and PCSK5 play a role in organizing the actin cytoskeleton and cell polarity [45], [46]. The gene for the epithelial-specific Ets transcription factor ELF3 (also known as ESX), involved in mammary gland development [47], was highly expressed during acinar morphogenesis of *BRIP1*-knockdown cells (Table S1 and Fig. 3B). Consistent with this observation, *ELF3* is over-expressed at the early stage of development of ductal carcinoma in situ [48]. We also found down-regulation of genes encoding the adhesion-related molecules COL8A1 and MCAM in *BRIP1*-knockdown cells (Table 1 and Fig. 3B), similar to previous reports [49], [50]. The gene encoding WIPF1, a member of the WASP and WAVE family of proteins, and growth arrest–specific gene *GAS1* were also down-regulated (Table 1, Tables S2, S3 and Fig. 3B). The former is involved in organizing the actin cytoskeleton, cell-cell adhesion, and cell motility [51], and the latter is associated with the higher rate of proliferation (Fig. 1C and Fig. 2G). Taken together, dysregulation of these genes may, at least in part, be associated with the induction of the neoplastic-like changes of *BRIP1*-knockdown cells by the disruption of proper cell adhesion, polarity, growth, and differentiation.

Previously, BRCA1 and SATB1 were shown to be involved in acinar formation of mammary epithelial cells in 3D culture [22], [27], [44]. Analogous to the findings in the *BRCA1*-depleted and *SATB1*-overexpressed cells, abnormalities in acinar formation and proliferation were observed in *BRIP1*-knockdown cells. However, the groups of dysregulated genes in the *BRIP1*-knockdown cells did not coincide with those reported in the *BRCA1*-depleted cells [22], suggesting BRCA1-independent functions of BRIP1 in mammary gland morphogenesis. In support with this, it has been suggested that the majority of BRIP1 exists in a native complex without BRCA1 [18]. On the other hands, it would be interesting as a future study to further investigate the physical interaction between BRIP1 and BRCA1 by comparing side by side the phenotype and dysregulation of genes in single- and double-knockdown cells of both proteins. In contrast, the major downstream signaling of SATB1 involving cell adhesion, polarity, growth and phosphatidylinositol signaling [27] was dysregulated in *BRIP1*-knockdown cells.

In the present study, we further investigated the tumorigenic potential of BRIP1-depleted cells *in vivo*. These cells, which were transplanted into mammary fat pads, did not develop into tumor in nude mice. This result indicates that loss of BRIP1 alone is insufficient to induce tumor formation. This may be related to the fact that BRIP1 is categorized as a moderate risk gene for breast cancer. However, it remains to be established whether the complete inactivation of BRIP1 could induce malignancy. Recently, Ordinario *et al* reported that ATM suppresses SATB1-induced malignant phenotypes of MCF-10A cells [44]. Since our microarray analysis showed an activation of ATM signaling pathway in *BRIP1*-knockdown cells, a part of SATB 1-mediated signaling events for full malignancy may be prevented by ATM in these cells.

In conclusion, the present findings suggest critical roles of BRIP1 helicase in mammary gland development by affecting multiple cellular signaling pathways, and provide a possible mechanism to explain how BRIP1 deficiency contributes to breast tumorigenesis.

Supporting Information

Figure S1 Morphological change in the *BRIP1*-knockdown mammary epithelial cells. Phase-contrast images of the non-target shRNA–transduced (**A**, **B**) and the *BRIP1* shRNA–transduced (**C**, **D**) cells in conventional 2D culture. Scale bars, 50 μm.
(TIF)

Figure S2 Expression profiling of the *BRIP1*-knockdown mammary epithelial cells. (**A**) Principal component analysis distinguished the *BRIP1* shRNA–transduced cells from the non-target shRNA–transduced cells on the basis of their expression profiles. (**B**) Distribution of the GO biological processes in the dysregulated genes in 3D culture of the *BRIP1*-knockdown mammary epithelial cells. Genes that were significantly up- or down-regulated in cells transduced with the *BRIP1*-specified shRNA compared with those transduced with the non-target shRNA are categorized by their GO biological processes.
(TIF)

Table S1 Up- and down-regulated genes (≥2-fold, $P<0.05$) in 3D culture of BRIP1-knockdown cells compared with control cells at day 4.
(PDF)

Table S2 Up- and down-regulated genes (≥2-fold, $P<0.05$) in 3D culture of BRIP1-knockdown cells compared with control cells at day 8.
(PDF)

Table S3 Up- and down-regulated genes (≥2-fold, $P<0.05$) in 3D culture of BRIP1-knockdown cells compared with control cells at day 12.
(PDF)

Table S4 Gene Set Enrichment Analysis (GSEA) gene sets positively or negatively correlated with 3D cultured BRIP1-knockdown cells compared with control cells.
(PDF)

Table S5 Oligonucleotide sequences used for quantitative RT-PCR.
(PDF)

Methods S1 DNA microarray data analysis.
(DOC)

Acknowledgments

We thank our laboratory members for research assistance and the Laboratory Animal and Genome Sciences Section for animal management.

Author Contributions

Conceived and designed the experiments: KD TI DI MN YS. Performed the experiments: KD. Analyzed the data: KD TM ST. Contributed reagents/materials/analysis tools: DI. Wrote the paper: KD TI YS.

References

1. Easton DF (1999) How many more breast cancer predisposition genes are there? Breast Cancer Res. 1; 14–17.
2. Ponder BA, Antoniou A, Dunning A, Easton DF, Pharoah PD (2005) Polygenic inherited predisposition to breast cancer. Cold Spring Harb Symp Quant Biol 70; 35–41.
3. Szabo CI, King MC (1997) Population genetics of BRCA1 and BRCA2. Am J Hum Genet 60; 1013–1020.
4. Antoniou A, Pharoah PD, Narod S, Risch HA, Eyfjord JE, et al. (2003) Average risks of breast and ovarian cancer associated with BRCA1 or BRCA2 mutations detected in case Series unselected for family history: a combined analysis of 22 studies. Am J Hum Genet 72; 1117–1130.
5. Serova OM, Mazoyer S, Puget N, Dubois V, Tonin P, et al. (1997) Mutations in BRCA1 and BRCA2 in breast cancer families: are there more breast cancer-susceptibility genes? Am J Hum Genet 60; 486–495.
6. Schubert EL, Lee MK, Mefford HC, Argonza RH, Morrow JE, et al. (1997) BRCA2 in American families with four or more cases of breast or ovarian cancer: recurrent and novel mutations, variableexpression, penetrance, and the possibility of families whose cancer is not attributable to BRCA1 or BRCA2. Am J Hum Genet 60; 1031–1040.
7. Peto J, Collins N, Barfoot R, Seal S, Warren W, et al. (1999) Prevalence of BRCA1 and BRCA2 gene mutations in patients with early-onset breast cancer. J Natl Cancer Inst 91; 943–949.
8. Seal S, Thompson D, Renwick A, Elliott A, Kelly P, et al. (2006) Truncating mutations in the Fanconi anemia J gene BRIP1 are low-penetrance breast cancer susceptibility alleles. Nat Genet 38; 1239–1241.
9. Byrnes GB, Southey MC, Hopper JL (2008) Are the so-called low penetrance breast cancer genes, ATM, BRIP1, PALB2 and CHEK2, high risk for women with strong family histories? Breast Cancer Res 10; 208.
10. Cantor SB, Bell DW, Ganesan S, Kass EM, Drapkin R, et al. (2001) BACH1, a novel helicase-like protein, interacts directly with BRCA1 and contributes to its DNA repair function. Cell 105; 149–160.
11. Yu X, Chini CC, He M, Mer G, Chen J (2003) The BRCT domain is a phospho-protein binding domain. Science 302; 639–642.
12. Cantor S, Drapkin R, Zhang F, Lin Y, Han J, et al. (2004) The BRCA1-associated protein BACH1 is a DNA helicase targeted by clinically relevant inactivating mutations. Proc Natl Acad Sci U S A 101; 2357–2362.
13. Peng M, Litman R, Jin Z, Fong G, Cantor SB (2006) BACH1 is a DNA repair protein supporting BRCA1 damage response. Oncogene 25; 2245–2253.
14. Tu Z, Aird KM, Bitler BG, Nicodemus JP, Beeharry N, et al. (2011) Oncogenic Ras Regulates BRIP1 Expression to Induce Dissociation of BRCA1 from Chromatin, Inhibit DNA Repair, and Promote Senescence. Dev Cell 21; 1077–1091.
15. Phelan CM, Borg A, Cuny M, Crichton DN, Baldersson T, et al. (1998) Consortium study on 1280 breast carcinomas: allelic loss on chromosome 17 targets subregions associated with family history and clinical parameters. Cancer Res 58; 1004–1012.
16. Callahan R (1998) Somatic mutations that contribute to breast cancer. Biochem Soc Symp 63; 211–221.
17. Cantor SB, Guillemette S (2011) Hereditary breast cancer and the BRCA1-associated FANCJ/BACH1/BRIP1. Future Oncol 7; 253–261.
18. De Nicolo A, Tancredi M, Lombardi G, Flemma CC, Barbuti S, et al. (2008) A novel breast cancer-associated BRIP1 (FANCJ/BACH1) germ-line mutation impairs protein stability and function. Clin Cancer Res 14; 4672–4680.
19. Deng CX, Wang RH (2003) Roles of BRCA1 in DNA damage repair: a link between development and cancer. Hum Mol Genet 12; R113–123.
20. Phillips ER, McKinnon PJ (2007) DNA double-strand break repair and development. Oncogene 26; 7799–7808.
21. Xu X, Wagner KU, Larson D, Weaver Z, Li C, et al. (1999) Conditional mutation of Brca1 in mammary epithelial cells results in blunted ductal morphogenesis and tumour formation. Nat Genet 22; 37–43.
22. Furuta S, Jiang X, Gu B, Cheng E, Chen PL, et al. (2005) Depletion of BRCA1 impairs differentiation but enhances proliferation of mammary epithelial cells. Proc Natl Acad Sci U S A 102; 9176–9181.
23. Debnath J, Muthuswamy SK, Brugge JS (2003) Morphogenesis and oncogenesis of MCF-10A mammary epithelial acini grown in three-dimensional basement membrane cultures. Methods 30; 256–268.
24. Ishida Y, Takabatake T, Kakinuma S, Doi K, Yamauchi K, et al. (2010) Genomic and gene expression signatures of radiation in medulloblastomas after low-dose irradiation in Ptch1 heterozygous mice. Carcinogenesis 31; 1694–1701.
25. Mootha VK, Lindgren CM, Eriksson KF, Subramanian A, Sihag S, et al. (2003) PGC-1alpha-responsive genes involved in oxidative phosphorylation are coordinately downregulated in human diabetes. Nat Genet 34; 267–273.
26. Subramanian A, Tamayo P, Mootha VK, Mukherjee S, Ebert BL, et al. (2005) Gene set enrichment analysis: a knowledge-based approach for interpreting genome-wide expression profiles. Proc Natl Acad Sci U S A 102; 15545–15550.
27. Han HJ, Russo J, Kohwi Y, Kohwi-Shigematsu T (2008) SATB1 reprogrammes gene expression to promote breast tumour growth and metastasis. Nature 452; 187–193.
28. Contos JJ, Ishii I, Chun J (2000) Lysophosphatidic acid receptors. Mol Pharmacol 58; 1188–1196.
29. Moolenaar WH, van Meeteren LA, Giepmans BN (2004) The ins and outs of lysophosphatidic acid signaling. Bioessays 26; 870–881.
30. Kitayama J, Shida D, Sako A, Ishikawa M, Hama K, et al. (2004) Over-expression of lysophosphatidic acid receptor-2 in human invasive ductal carcinoma. Breast Cancer Res 6; R640–646.
31. Liu S, Umezu-Goto M, Murph M, Lu Y, Liu W, et al. (2009) Expression of autotaxin and lysophosphatidic acid receptors increases mammary tumorigenesis, invasion, and metastases. Cancer Cell 15; 539–550.
32. Chen Y, Olopade OI (2008) MYC in breast tumor progression. Expert Rev Anticancer Ther 8; 1689–1698.
33. Xu J, Chen Y, Olopade OI (2010) MYC and Breast Cancer. Genes Cancer 1; 629–640.
34. Boras-Granic K, Wysolmerski JJ (2008) Wnt signaling in breast organogenesis. Organogenesis 4; 116–122.
35. Roy R, Chun J, Powell SN (2012) BRCA1 and BRCA2: different roles in a common pathway of genome protection. Nat Rev Cancer 12; 68–78.
36. Gorgoulis VG, Vassiliou LV, Karakaidos P, Zacharatos P, Kotsinas A, Liloglou T, et al. (2005) Activation of the DNA damage checkpoint and genomic instability in human precancerous lesions. Nature 434; 907–913.
37. Bartkova J, Horejsi Z, Koed K, Kramer A, Tort F, et al. (2005) DNA damage response as a candidate anti-cancer barrier in early human tumorigenesis. Nature 434; 864–870.
38. Halazonetis TD, Gorgoulis VG, Bartek J (2008) An oncogene-induced DNA damage model for cancer development. Science 319; 1352–1355.
39. Cully M, You H, Levine AJ, Mak TW (2006) Beyond PTEN mutations: the PI3K pathway as an integrator of multiple inputs during tumorigenesis. Nat Rev Cancer 6; 184–192.
40. Fournier MV, Fata JE, Martin KJ, Yaswen P, Bissell MJ (2009) Interaction of E-cadherin and PTEN regulates morphogenesis and growth arrest in human mammary epithelial cells. Cancer Res 69; 4545–4552.
41. Liu H, Radisky DC, Wang F, Bissell MJ (2004) Polarity and proliferation are controlled by distinct signaling pathways downstream of PI3-kinase in breast epithelial tumor cells. J Cell Biol 164; 603–612.
42. Isakoff SJ, Engelman JA, Irie HY, Luo J, Brachmann SM, et al. (2005) Breast cancer-associated PIK3CA mutations are oncogenic in mammary epithelial cells. Cancer Res 65; 10992–11000.
43. Patani N, Jiang W, Mansel R, Newbold R, Mokbel K (2009) The mRNA expression of SATB1 and SATB2 in human breast cancer. Cancer Cell Int 9; 18.
44. Ordinario E, Han HJ, Furuta S, Heiser LM, Jakkula LR, et al. (2012) ATM Suppresses SATB1-Induced Malignant Progression in Breast Epithelial Cells. PLoS One 7; e51786.
45. Rollason R, Korolchuk V, Hamilton C, Jepson M, Banting G (2009) A CD317/tetherin-RICH2 complex plays a critical role in the organization of the subapical actin cytoskeleton in polarized epithelial cells. J Cell Biol 184; 721–736.
46. Heng S, Cervero A, Simon C, Stephens AN, Li Y, et al. (2011) Proprotein convertase 5/6 is critical for embryo implantation in women: regulating receptivity by cleaving EBP50, modulating ezrin binding, and membrane-cytoskeletal interactions. Endocrinology 152; 5041–5052.
47. Neve R, Chang CH, Scott GK, Wong A, Friis RR, et al. (1998) The epithelium-specific ets transcription factor ESX is associated with mammary gland development and involution. FASEB J 12; 1541–1550.
48. Chang CH, Scott GK, Kuo WL, Xiong X, Suzdaltseva Y, et al. (1997) ESX: a structurally unique Ets overexpressed early during human breast tumorigenesis. Oncogene 14; 1617–1622.
49. Cechowska-Pasko M, Palka J, Wojtukiewicz MZ (2006) Enhanced prolidase activity and decreased collagen content in breast cancer tissue. Int J Exp Pathol 87; 289–296.
50. Shih LM, Hsu MY, Palazzo JP, Herlyn M (1997) The cell-cell adhesion receptor Mel-CAM acts as a tumor suppressor in breast carcinoma. Am J Pathol 151; 745–751.
51. Kurisu S, Takenawa T (2009) The WASP and WAVE family proteins. Genome Biol 10; 226.

RADIATION RESEARCH 180, 439–447 (2013)
0033-7587/13 $15.00

DOI: 10.1667/RR13351.1

COMMENTARY

Measurements of Individual Radiation Doses in Residents Living Around the Fukushima Nuclear Power Plant

Shigenobu Nagataki,[a,b] Noboru Takamura,[c,1] Kenji Kamiya[d,e] and Makoto Akashi[f]

[a] *Nagasaki University (Emeritus Professor), 1-12-4 Sakamoto, Nagasaki City, 852-8523,* [b] *Radiation Effects Research Foundation (Past Chairman), 5-2 Hijiyama Park, Minami-ku, Hiroshima, 732-0815,* [c] *Department of Global Health, Medicine and Welfare, Atomic Bomb Disease Institute, Nagasaki University, 1-12-4 Sakamoto, Nagasaki 852-8523,* [d] *Research Institute for Radiation Biology and Medicine, Hiroshima University, 1-2-3 Kasumi, Minami-ku, Hiroshima 734-8553,* [e] *Radiation Medical Science Center for the Fukushima Health Management Survey, Fukushima Medical University, Hikarigaoka 1, Fukushima 960-1295,* [f] *National Institute of Radiological Sciences, 4-9-1 Anagawa, Inage-ku, Chiba 263-8555, Japan*

Nagataki, S., Takamura, N., Kamiya, K. and Akashi, M. Measurements of Individual Radiation Doses in Residents Living Around the Fukushima Nuclear Power Plant. *Radiat. Res.* 180, 439–447 (2013).

At the outset of the accident at Fukushima Daiichi Nuclear Power Plant in March 2011, the radiation doses experienced by residents were calculated from the readings at monitoring posts, with several assumptions being made from the point of view of protection and safety. However, health effects should also be estimated by obtaining measurements of the individual radiation doses. The individual external radiation doses, determined by a behavior survey in the "evacuation and deliberate evacuation area" in the first 4 months, were <5 mSv in 97.4% of residents (maximum: 15 mSv). Doses in Fukushima Prefecture were <3 mSv in 99.3% of 386,572 residents analyzed. External doses in Fukushima City determined by personal dosimeters were <1 mSv/3 months (September–November, 2011) in 99.7% of residents (maximum: 2.7 mSv). Thyroid radiation doses, determined in March using a NaI (Tl) scintillation survey meter in children in the evacuation and deliberate evacuation area, were <10 mSv in 95.7% of children (maximum: 35 mSv). Therefore, all doses were less than the intervention level of 50 mSv proposed by international organizations. Internal radiation doses determined by cesium-134 (^{134}C) and cesium-137 (^{137}C) whole-body counters (WBCs) were <1 mSv in 99% of the residents, and the maximum thyroid equivalent dose by iodine-131 WBCs was 20 mSv. The exploratory committee of the Fukushima Health Management Survey mentions on its website that radiation from the accident is unlikely to be a cause of adverse health effects in the future. In any event, sincere scientific efforts must continue to obtain individual radiation doses that are as accurate as possible. However, observation of the health effects of the radiation doses described above will require reevaluation of the protocol used for determining adverse health effects. The dose-response relationship is crucial, and the aim of the survey should be to collect sufficient data to confirm the presence or absence of radiation health effects. In particular, the schedule of decontamination needs reconsideration. The decontamination map is determined based on the results of airborne monitoring and the radiation dose calculated from readings taken at the monitoring posts at the initial period of the accident. The decontamination protocol should be reevaluated based on the individual doses of the people who desire to live in those areas.

[1]Address for correspondence: Department of Global Health, Medicine and Welfare, Atomic Bomb Disease Institute, Nagasaki University, 1-12-4 Sakamoto, Nagasaki 852-8523, Japan; e-mail: takamura@nagasaki-u.ac.jp.

INTRODUCTION

More than two years have passed since the accident at the Fukushima Daiichi Nuclear Power Plant, but scientific information on that accident has not yet been compiled (*1–4*). The assessment of radiation doses in the general population in Fukushima is important for evaluating the scale of the accident as well as the effectiveness of countermeasures taken by the local and central Japanese governments. In addition, the results of this assessment provide important and fundamental information for preparing future countermeasures. Radiation doses in the initial period after the accident were calculated from simple readings taken at monitoring points using several assumptions with respect to protection and safety. Information about individual radiation doses should be used immediately to estimate the health effects of radiation.

Various research institutes have reported (in Japanese) measurements of individual radiation doses of residents surrounding the Fukushima Daiichi Nuclear Power Plant at various times and places since the accident. Each research institute will present formal reports in English at a later date, but we, as members of Japanese scientific societies, have

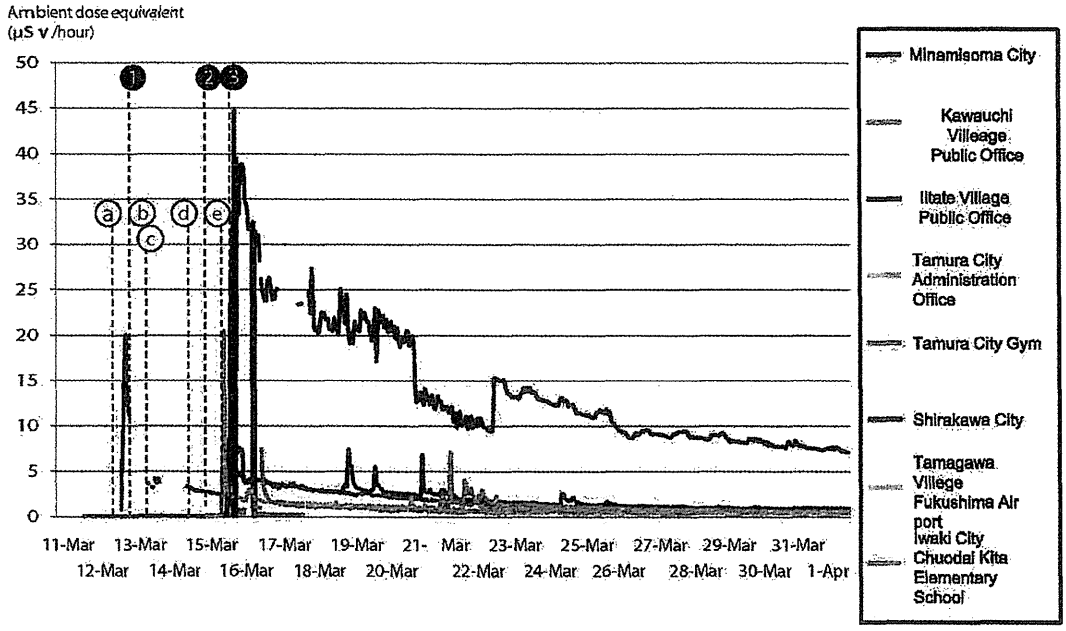

FIG. 1. The ambient dose equivalent around the nuclear power plant at the initial phase of the accident, recorded by monitoring devices that were not damaged by the earthquake or tsunami. The location of each city and village is indicated in Fig. 2a. 1. Hydrogen explosion at unit 1 at 15:36, March 12, 2011; 2. Hydrogen explosion at unit 3 at 11:01, March 14, 2011; 3. Hydrogen explosion at unit 4 at 06:14, March 15, 2011; a. Vent opened at unit 1 at 10:17, March 12, 2011; b. Vent opened at unit 3 at 08:41, March 13, 2011; c. Vent opened at unit 2 at 11:00, March 13, 2011; d. Vent opened at unit 3 at 05:20, March 14, 2011; and e. Vent opened at unit 2 at 00:02, March 15, 2011.

reviewed reports (mainly located on Japanese websites) on the estimation and the actual measurement of the individual radiation doses in residents. In this article, we present a brief summary of these measurements to worldwide specialists in the field of radiation research.

OUTLINE OF THE ACCIDENT AND ITS COUNTERMEASURES

On March 11, 2011, a 9.0-magnitude earthquake (the Great East Japan Earthquake) struck the east coast of Japan near Iwate, Miyagi and Fukushima Prefectures. Fifty minutes after the earthquake, a tsunami with a height over 15 m hit the Fukushima Daiichi Nuclear Power Plant, causing extensive damage to its cooling system and resulting in the loss of all power sources at the plant (*4*). Consequently, a radioactive plume from units 1–4 was dispersed into the atmosphere. Figure 1 shows the dose rates around the nuclear power plant at the initial phase of the accident, which were recorded by monitoring devices that had not been damaged by the earthquake or tsunami.

Instructions to evacuate or remain inside were issued to the local residents by the Director-General (Prime Minister) of the Nuclear Emergency Response Headquarters. This office was established on March 11, 2011, within the Cabinet of Japan, to organize this emergency response: At 20:50 on that day, residents who lived within a 2-km radius of the plant were told to evacuate. This order was extended to a 3-km radius at 21:23 on that day, then to a 10-km radius on the morning of March 12, and then to a 20-km radius that afternoon. On March 14, Fukushima Prefecture performed ambient dose monitoring, and on March 15, those living within 20–30 km were instructed to take shelter inside their houses (*5*). On March 17, the government initiated "food control" to minimize internal radiation exposure, and all contaminated cow's milk was disposed of. These decisions resulted in the evacuation of almost 110,000 people after the accident.

On April 22, 2011, the government designated a "deliberate evacuation area" where the annual cumulative radiation dose was predicted to reach 20 mSv (*5*). Chronological events during the initial phase of the accident are shown in Table 1. Many issues are currently being discussed, such as decontamination, health check-ups and the return of the population. To date, no victims or patients with acute radiation syndrome have been reported in the general population or among workers in the nuclear power plants.

ESTIMATION OF INDIVIDUAL EXTERNAL RADIATION DOSE FROM A BEHAVIOR SURVEY

The Fukushima Health Management Survey conducted by Fukushima Prefecture estimated the external radiation

TABLE 1
Chronological Events During the Initial Phase of the Accident at the FNPP

Date	Nuclear power plant accident/evacuation Orders/evacuation	Implemented policies on food control
March 11	20:50 – Evacuation order for residents within a 2-km radius	
	21:23 – Evacuation order within a 3-km radius	
	21:23 – Sheltering order within a 3–10-km radius	
March 12	0:30 – Complete evacuation of residents within a 3-km radius	
	5:44 – Evacuation instructions within a 10-km radius	
	15:36 – **Unit 1: Hydrogen explosion**	
	18:25 – Evacuation order within a 20-km radius	
March 14	11:01 – **Unit 3: Hydrogen explosion**	
March 15	6:14 – **Unit 2: suppression chamber: Hydrogen explosion – Unit 4: Hydrogen explosion**	
	10:00 – Evacuation of Namie Town recommended	
	11:00 – Sheltering order within a 20–30-km radius	
	14:00 – **Complete evacuation of residents within a 20-km radius**	
March 17		**Establishment of provisional regulation values for ^{131}I (300 Bq/kg for drinking water and milk and 2,000 Bq/kg for vegetables, respectively), ^{134}Cs and ^{137}Cs (200 Bq/kg for drinking water and milk, 500 Bq/kg for vegetables, grains and meats, fishes and eggs, respectively).**
March 21		**Order to restrict shipping of food products exceeding provisional regulation values (hereafter, shipping restricted on products exceeding regulation values).**
March 25	11:46 – Chief Cabinet Secretary announced an active voluntary evacuation of residents within a 20–30-km radius	
April 22	**Establishment of a deliberate evacuation area and restricted area**	

dose of residents based on their behavior. The National Institute of Radiological Sciences (NIRS) developed an external radiation evaluation system that estimated individual external radiation doses using two types of information collected during the 4 months after the accident (March 11 to July 11, 2011). Information was gathered about residents' behaviors within their dwellings and other places that they visited, their modes of transportation, times of occupancy (indoor, outdoor), and the ambient dose equivalent monitored by the government and other related organizations (*6*).

On January 25, 2012, at their fifth reviewing board meeting, the Fukushima Prefectural Health Survey announced the provision of results for the individual external dose for 1,727 residents in the evacuation and deliberate evacuation areas to residents on December 13, 2011: 65 residents were from Iitate Village, 228 from Kawamata Town and 1,296 from Namie Town. Of these, 1,589 were not radiation workers (*6*). Among these 1,589 residents from the evacuation areas, 987 (62.8%) received <1 mSv; 1,335 (85.8%) received <2 mSv; 1,464 (93.9%) received <3 mSv; and 1,518 (97.4%) received <5 mSv. The maximum dose was 15 mSv (Fig. 2). The survey committee concluded from these radiation doses that health effects are unlikely to appear in the future (*7, 8*).

In February 2013, Fukushima Prefecture summarized the results of questionnaire responses from 477,121 out of 2,056,994 residents (23.3%) who resided in Fukushima Prefecture at the time of the accident. These results indicated that 256,281 (66.3%) of the residents had exposures <1 mSv, 367,175 (95.0%) had <2 mSv and 383,901 (99.3%) had <3 mSv (*9*) (Fig. 3).

MEASUREMENTS OF INDIVIDUAL EXTERNAL EXPOSURE USING A PERSONAL DOSIMETER

The measured individual external doses of Fukushima residents, obtained from personal dosimeter readings, are summarized in Table 2. The categories included the type of personal dosimeter and its sensitivity, measurement period, number and age of residents surveyed, and dose range. Each city reported a dose range by different summary methods.

Two types of personal dosimeters were used in each city: the Glass Badge® (Chiyoda Technol Corp.) was used in Fukushima City and Date City. While the Quixel Badge® (Nagase Landauer, LTD) was used in Nihonmatsu City, Tamura City and Koriyama City. The measurement principle behind the Glass Badge® is radio photoluminescence, while the Quixel Badge® uses optically stimulated

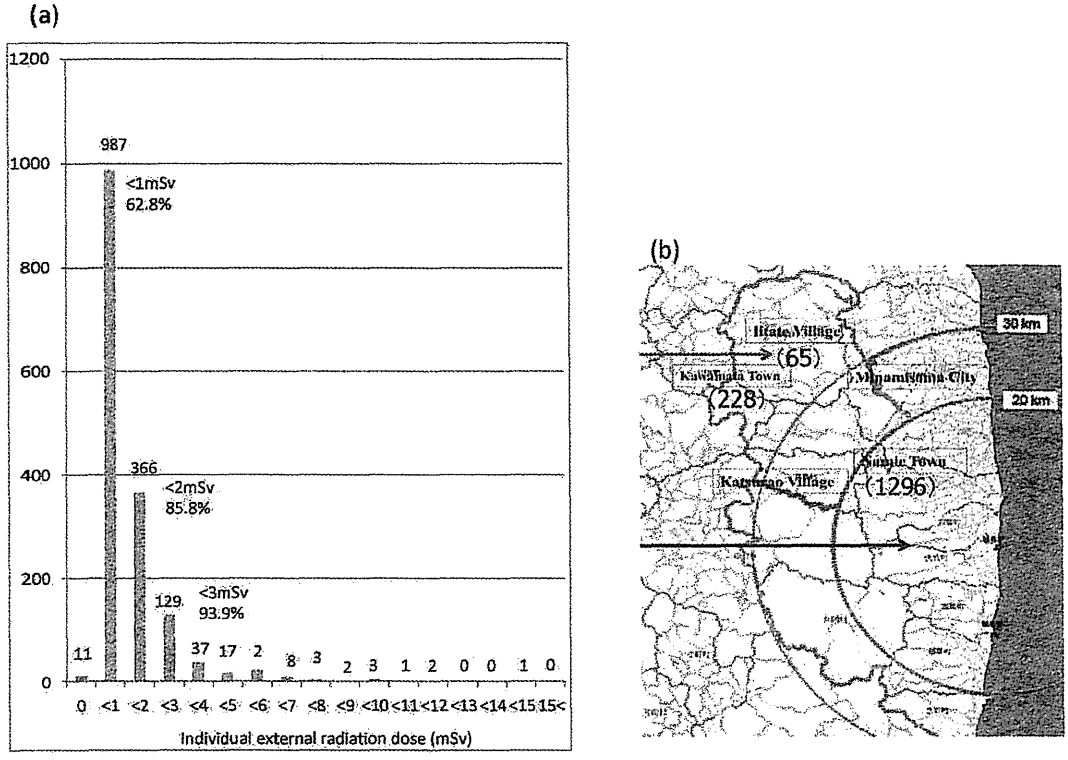

FIG. 2. Individual external radiation doses in the "evacuation" and "deliberate evacuation" areas during the first 4 months (panel a). The number of people examined in each village or town is indicated in panel b.

luminescence; the measurement limit of both types is 0.01 mSv.

In Fukushima City, personal dosimeters were distributed to infants, elementary and junior high school students and pregnant women. The measurement period was 3 months, from September 1 to November 30, 2011. The individual accumulated external dose for a three-month period was obtained for 36,767 people. Fukushima reported the frequency distribution of accumulated doses in its residents as follows: 87.2% of surveyed residents received doses of

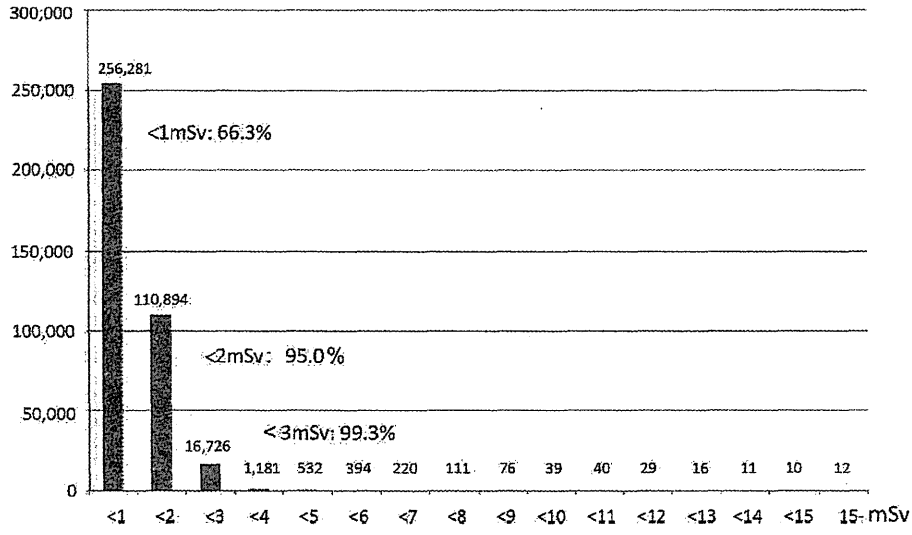

FIG. 3. Individual external radiation doses in Fukushima Prefecture. From a total of 2,056,994 subjects, 477,121 (23.2%) responded and 386,572 subjects who were nonradiation workers were analyzed.

TABLE 2
The Individual External Exposure Dose of the Residents in Fukushima Measured by Personal Dosimeters

City	Personal dosimeter: Maker	Personal dosimeter: Sensitivity	Measurement period	Number of residents surveyed	Age group	Dose range (frequency/districts/age group)
Fukushima	Chiyoda Technol Corp. Glass Badge®	≥0.01 mSv	September 1 –November 30, 2011 (3 months)	36,767	Junior high school students and below, as well as pregnant women	Frequency distribution, accumulated dose (3 months) (D mSv) D < 0.1 mSv: 9.0% 0.1 ≦ D < 0.5 mSv: 78.2% 0.5 ≦ D < 1.0 mSv: 12.5% 1.0 ≦ D < 1.5 mSv: 0.25% 1.5 ≦ D < 2.0 mSv: 0.027% 2.0 ≦ D < 2.5 mSv: 0.005% 2.5 ≦ D < 3.0 mSv: 0.014%
Date (*10*)	Chiyoda Technol Corp. Glass Badge®	≥0.01 mSv	September 1 –November 30, 2011 (3 months)	9,443	All ages	District, average accumulated dose (3 months) Ryozen district: 0.71 mSv Tsukidate district: 0.43 mSv Hobara district: 0.31 mSv Date district: 0.20 mSv Yanagawa district: 0.17 mSv 0.3% (33 persons), ≧ 10 mSv/year 2 persons, ≧ 20 mSv/year
Nihonmatsu (*11*)	Nagase Landauer, LTD Quixel Badge®	≥0.01 mSv	September 1 –November 30, 2011 (3 months)	8,725	0–6 years: 2,096	Age group, average accumulated dose (3 months) 0–6 years: 0.41 mSv
					Elementary School: 3,158	Elementary school: 0.37 mSv
					Junior high School: 1,654	Junior high school: 0.37 mSv
					High School: 703	High school: 0.41 mSv
					19–40 years (female): 1,079	19–40 years (female): 0.38 mSv
					Other students: 35	Other students: 0.28 mSv
Tamura (*12*)	Nagase Landauer, LTD Quixel Badge®	≥0.01 mSv	September 30, 2011 –January 10, 2012 (103 days)	4,559	Junior high school and below, as well as pregnant women	District (persons), average accumulated dose (103 days) Takine (626): 0.10 mSv Ohgoe (509): 0.10 mSv Miyakoji (302): 0.17 mSv Tokiwa (734): 0.16 mSv Funehiki (2,468): 0.15 mSv
Koriyama (*13*)	Nagase Landauer, LTD Quixel Badge®	≥0.01 mSv	November 7, 2011 –January 9, 2012 (64 days)	24,115	Elementary school / Junior high school	Frequency distribution, accumulated dose (64 days) Highest 1.31 mSv / Lowest 0.01 mSv / Average 0.17 mSv 0.01–0.09 mSv: 21.7% 0.10–0.19 mSv: 41.7% 0.20–0.29 mSv: 28.4% 0.30–0.39 mSv: 6.5% 0.40–0.49 mSv: 1.2% 0.50– : 0.37%

<0.5 mSv/3 months and 99.7% received <1 mSv/3 months. Cases where values exceeded 2 mSv were determined to be results of inappropriate use of the badges (e.g., placed outdoors, left on bicycles or put through X-ray inspection during baggage checks at the airport).

Date City and Tamura City totaled the personal accumulated doses of their residents according to district. Date City's measurements were obtained over 3 months and reported as accumulated doses for residents of each district. The dose was lowest in Yanagawa district (0.17 mSv) and highest in Ryozen district (0.71 mSv) (*10*). Nihonmatsu City reported the accumulated doses over 3 months by age groups (i.e., elementary school students, junior high school students, etc.), with a dose range of 0.28–0.41 mSv (*11*). Tamura City measured the personal accumulated doses for 103 days, with a dose range from 0.10 mSv at Ohgoe and

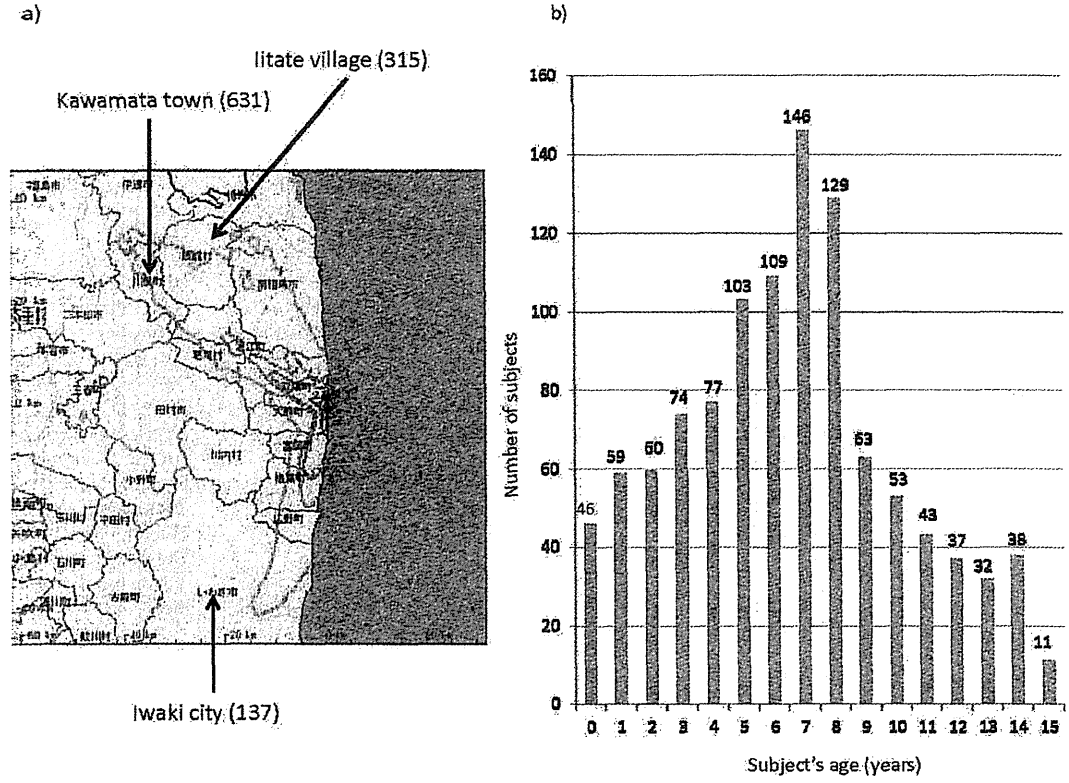

FIG. 4. Screening survey on thyroid exposure for children performed from March 26–30, 2011, by the Nuclear Emergency Response Headquarter and NIRS, indicated with the thyroid equivalent dose evaluated by SPEEDI system. The thyroid dose was calculated using the internal dose coefficients currently available from International Commission on Radiological Protection (ICRP) publication 72 and the age-dependent thyroid mass. We used a systemic model for iodine (ICRP publication 56) and general models of the respiratory tract for inhalation (ICRP publication 66). The dose estimation was also based on a scenario of chronic intake via inhalation from March 12, 2011, to the day before the measurement day. Panel a: the numbers in the parentheses indicates the number of people examined in each village or town and the age distribution of children is shown in panel b.

Takine to 0.17 mSv at Miyakoji (*12*). Koriyama City reported a frequency distribution for its residents with accumulated doses for 64 days; 91.89% of those surveyed had a dose range of 0.01–0.29 mSv (*13*).

Fukushima Prefecture announced the results of measurements made using personal dosimeters in its 22 municipalities, omitting the names of cities, towns or villages for reasons of personal information protection (*14*). The prefecture indicated that the median reported values were <1 mSv/year.

RADIATION DOSE TO THYROID GLANDS IN CHILDREN

The SPEEDI system suggested that the thyroid equivalent dose might have reached 100 mSv in hypothetical one-year-old children in some areas, based on the assumption of a continuous intake of contaminated foods from March 12–24, 2011. Thus, evaluation of the thyroid dose was urgent for residents in these areas.

The unavailability of thyroid monitors meant that an alternative thyroid monitoring method, using a NaI (Tl) scintillation survey meter, was used for ambient dose rate measurements. This test was performed from March 26–30, 2011.

Overall, 315 children ranging from 0–15 years of age from Iitate Village, 631 from Kawamata Town, and 137 from Iwaki City participated in the survey. The number of children are shown in Fig. 4a and the age distribution of these children is shown in Fig. 4b. Figure 5 shows the distribution of thyroid equivalent doses estimated from the screening survey and intake scenario from March 12, 2011, to the day before measurement: 95.7% of the children received <10 mSv, with a maximum of 35 mSv, which is lower than the intervention level (50 mSv) (*15, 16*). In Fig. 6, these values are compared to those of the dose-response relationship between thyroid cancer and iodine-131 (^{131}I) in the Ukraine and Belarus as a result of the Chernobyl accident (*17, 18*). Values for Fukushima are shown on the red line in the figures.

In a separate project, Tokonami *et al.* conducted ^{131}I-activity measurements of the thyroid glands of 62 residents and evacuees during the period from April 12–16, 2011, by placing a NaI (Tl) scintillation spectrometer